INSTITUTE OF PHYSICS PUBLISHING REPORTS ON PROGRESS IN PHYSICS

Rep. Prog. Phys. **65** (2002) 1331–1386 PII: S0034-4885(02)95815-X

The physics of traffic jams

Takashi Nagatani

Division of Thermal Science, Department of Mechanical Engineering, Shizuoka University, Hamamatsu 432-8561, Japan

Received 15 May 2002, in final form 16 July 2002
Published 13 August 2002
Online at stacks.iop.org/RoPP/65/1331

Abstract

Traffic flow is a kind of many-body system of strongly interacting vehicles. Traffic jams are a typical signature of the complex behaviour of vehicular traffic. Various models are presented to understand the rich variety of physical phenomena exhibited by traffic. Analytical and numerical techniques are applied to study these models. Particularly, we present detailed results obtained mainly from the microscopic car-following models. A typical phenomenon is the dynamical jamming transition from the free traffic (FT) at low density to the congested traffic at high density. The jamming transition exhibits the phase diagram similar to a conventional gas–liquid phase transition: the FT and congested traffic correspond to the gas and liquid phases, respectively. The dynamical transition is described by the time-dependent Ginzburg–Landau equation for the phase transition. The jamming transition curve is given by the spinodal line. The metastability exists in the region between the spinodal and phase separation lines. The jams in the congested traffic reveal various density waves. Some of these density waves show typical nonlinear waves such as soliton, triangular shock and kink. The density waves are described by the nonlinear wave equations: the Korteweg-de-Vries (KdV) equation, the Burgers equation and the Modified KdV equation. Subjects like the traffic flow such as bus-route system and pedestrian flow are touched as well. The bus-route system with many buses exhibits the bunching transition where buses bunch together with proceeding ahead. Such dynamic models as the car-following model are proposed to investigate the bunching transition and bus delay. A recurrent bus exhibits the dynamical transition between the delay and schedule-time phases. The delay transition is described in terms of the nonlinear map. The pedestrian flow also reveals the jamming transition from the free flow at low density to the clogging at high density. Some models are presented to study the pedestrian flow. When the clogging occurs, the pedestrian flow shows the scaling behaviour.

Contents

1. Introduction

The concepts and techniques of physics are being applied to such complex systems as transportation systems (Nagel *et al* 1999, Chowdhury *et al* 2000, Helbing 2001), stock markets (Kertesz and Kondor 1998, Mantegna and Stanley 1999) and biological systems (Kauffmann 1995). Physics, other sciences and technologies meet at the frontier area of interdisciplinary research. The scientific studies for traffic problems were started in 1935 (Greenshields 1935). In 1955, Lighthill and Whitham have presented the oldest and most popular macroscopic traffic model based on the fluid-dynamic theory. They have studied the traffic jam as a shock wave by treating traffic as an effectively one-dimensional compressible fluid. Prigogine *et al* (1960, 1971) have presented the gas-kinetic model based on the Boltzmann equation. In 1961, Newell has proposed the microscopic, optimal velocity model based on the assumption of a delayed adaptation of velocity. In 1976 and 1978, Musha and Higuchi have studied the noisy behaviour of traffic flow and have conjectured that the fluctuations of traffic current exhibit the so-called $1/f$ noise.

Although there were already some early pioneer's works like Lighthill and Whitham (1955) and Prigogine (1961), the papers of Biham *et al* (1992), Nagel and Schreckenberg (1992) and Kerner and Kohnhauser (1993) triggered the main activities in traffic physics. Then, an avalanche of publications started in various international physics journal. The development of the modern traffic theories is due to the availability of computer and the concepts and techniques of modern physics. Traffic is modelled as a system of interacting vehicles driven far from equilibrium. The traffic models exhibit a rich variety of physical phenomena such as the dynamical jamming transition, critical phenomena, metastability, self-organized criticality and nonlinear waves (soliton), etc.

For decades, the functional relations between the vehicle current and the vehicle density (so-called fundamental diagram) have highly attracted attention of traffic researchers. Figure 1 shows schematically the typical time-averaged local measurements of the density ρ and current (flow) q. At low densities, the traffic shows the linear dependence of the traffic current on the density. In contrast, at high densities, the traffic current decreases with increasing density. There are strong fluctuations of the current at high densities. The vehicles move freely at low densities, while the vehicles are in a congested state at high densities. Thus, with increasing

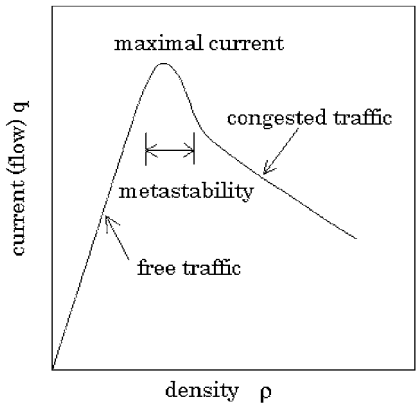

Figure 1. Schematic relationship (fundamental diagram) of the density ρ and current (flow) q. The vehicles move freely at low densities, while the vehicles are in a congested state at high densities. Near the maximal current, there is the metastable region.

vehicle density, the traffic state changes from the free traffic (FT) at low densities to the congested traffic at high densities. Near the density of the maximal current, the jamming transition from the FT to the congested traffic occurs. The jamming transition exhibits the hysteresis and metastability. The modern traffic theory has been developed to clarify the fundamental aspects of the jamming transition.

The traffic science aims to discover the fundamental properties and laws in transportation systems. On the other hand, traffic engineering aims at making the planning and implementation of the road network and control systems. In the traffic engineering area, the very complex traffic models have been proposed to forecast or estimate the traffic current in real transportation systems (Hurdle *et al* 1983, Daganzo 1993, 1997, Hall 1999). The models include so many factors that it is difficult to discover the essential factors affecting on the traffic behaviour. Physicists have proposed the simplified traffic models including a few factors at most to clarify the cause and effect. Despite the complexity of traffic and complications of human behaviour, physical traffic theory is an example of a highly quantitative description for a living system.

In this paper, we try to give an overview of traffic physics. Attention is paid to the formulation of the traffic dynamics, the dynamical phase transitions and the nonlinear waves. This paper is complimentary to those published in recent years by Chowdhury *et al* (2000) and Helbing (2001). The paper by Chowdhury *et al* (2000) discusses the methods and results for the cellular automaton models in great detail. Helbing's paper is mainly based on the gas-kinetic and macroscopic models. A large number of important papers on traffic published in recent years are based not only on CA and gas-kinetic models but also on the car-following models and fluid dynamic models. But the works of the car-following models have received little attention. Especially, the nonlinear wave equations describing the traffic jams have been sparsely discussed in the two papers. We discuss the methods and results for the car-following models in detail after explaining the traffic models and the micro–macro link. We focus on the dynamical phase transitions and the nonlinear density waves from the point of view of statistical physics and nonlinear waves. Also, we describe the linear stability theory in detail to explain the jamming transitions.

The outline of this paper is as follows. In section 2, we present the various traffic models where there are different conceptual frameworks for modelling traffic. In the macroscopic description, traffic is viewed as a compressible fluid. In the microscopic description, traffic is treated as a system of interacting particles driven far from equilibrium. We discuss the relationship between the microscopic model and the macroscopic model. In section 3, we discuss the stability of traffic flow and the jamming transition. The jamming transition is related to the linear instability. The jamming transition is described in terms of the time-dependent Ginzburg–Landau (TDGL) equation. The fundamental phase diagram of traffic is presented. It is shown that traffic exhibits similar behaviour to the phase transition and critical phenomenon in equilibrium systems. In section 4, we present the nonlinear wave equations describing the density waves appearing in traffic. The nonlinear wave equations are derived from the microscopic model. The distinct density waves appearing in the different regions of phase diagram are described by the different nonlinear wave equations. In section 5, the theoretical results are compared with the empirical data. The empirical data are explained in detail. It is shown that an agreement with empirical data is reached not only on a qualitative level but also on a quantitative level. In section 6, we present the microscopic models for bus-route systems. The bus-route models are the extended versions of traffic models. The bunching of buses is closely connected to the kinetic clustering of vehicle traffic. In section 7, we present the microscopic models of pedestrian flow. In the pedestrian flows, the jamming or clogging transitions also occur similarly to the traffic jams. Section 8 presents the summary.

2. Models of vehicular traffic

This section will give the various traffic models with different conceptual frameworks for modelling traffic. In the microscopic models, the traffic is treated as a system of interacting particles driven far from equilibrium. In contrast, in the so-called macroscopic models, the traffic is viewed as a compressible fluid.

2.1. Microscopic car-following models

The car-following model is a typical one of microscopic traffic models. The non-integer car-following models are called *follow-the-leader* models. The vehicle j is affected only by the vehicle ahead $j+1$, called the *leading* vehicle. Newell (1961) has proposed the *optimal velocity* model. The equation of motion for vehicle j is described as

$$\frac{\mathrm{d}x_j(t+\tau)}{\mathrm{d}t} = V(\Delta x_j(t)), \tag{1}$$

where $x_j(t)$ is the position of vehicle j at time t, τ is the delay time, $\Delta x_j(t)(= x_{j+1}(t) - x_j(t))$ is the headway of vehicle j at time t and $V(\Delta x_j(t))$ is the optimal velocity. The idea is that a driver adjusts the vehicle velocity according to the observed headway $\Delta x_j(t)$. The delay time τ allows for the time lag that it takes for the vehicle velocity to reach the optimal velocity $V(\Delta x_j(t))$ when the traffic flow is varying.

By using the Taylor-expanding equation (1), one obtains the differential equation model (Bando *et al* 1995a)

$$\frac{\mathrm{d}^2x_j(t)}{\mathrm{d}t^2} = \left(\frac{1}{\tau}\right)\left(V(\Delta x_j(t)) - \frac{\mathrm{d}x_j(t)}{\mathrm{d}t}\right). \tag{2}$$

The inverse $(1/\tau)$ of delay time is called the sensitivity a. By transforming the time derivative to the forward difference in equation (1), one obtains the difference equation model (Nagatani *et al* 1998, Nagatani 2000a)

$$x_j(t+2\tau) = x_j(t+\tau) + \tau V(\Delta x_j(t)). \tag{3}$$

It is useful to convert equation (3) to the headway equation:

$$\Delta x_j(t+2\tau) = \Delta x_j(t+\tau) + \tau[V(\Delta x_{j+1}(t)) - V(\Delta x_j(t))]. \tag{4}$$

The differential equation model (2) corresponds to the equation of motion of a mass with a simple friction:

$$m\frac{\mathrm{d}^2x_j(t)}{\mathrm{d}t^2} + \gamma\frac{\mathrm{d}x_j(t)}{\mathrm{d}t} = F(\Delta x_j(t)), \tag{5}$$

where m is the mass of a vehicle, γ is the friction coefficient of a vehicle and $F(\Delta x_j(t))$ is the driving force to accelerate or decelerate the vehicle. The delay time τ is given by m/γ. The optimal velocity $V(\Delta x_j(t))$ is connected to $F(\Delta x_j(t))/\gamma$.

Generally, it is necessary that the optimal velocity function has the following properties: it is a monotonically increasing function and it has an upper bound (maximal velocity). Bando *et al* (1995) suggest the relation

$$V(\Delta x_j(t)) = \frac{v_{\max}}{2}\{\tanh(\Delta x_j(t) - x_c) + \tanh(x_c)\}, \tag{6}$$

where x_c is a constant representing the safety distance. When $\Delta x_j \to \infty$ and $x_c > 0$, $V(\infty) \cong v_{\max}$. Equation (6) has a turning point (inflection point) at $\Delta x_j = x_c$. It is important that the optimal velocity function has the turning point. Otherwise, one cannot obtain a robust density wave representing a traffic jam.

The optimal velocity model is simple and convenient for computer simulation and theoretical analysis. As the optimal velocity model does not take into account a driver response to the relative velocity with respect to the vehicle ahead, it produces a collision accident with increasing delay τ. To avoid this collision, Treiber *et al* (1999a, 2000) have proposed the intelligent driver model (IDM) taking into account the relative velocity. Also, the relative velocity has been taken into account in some models (Gipps 1981, Krauss *et al* 1996, 1997, Helbing 1997a, Helbing and Tilch 1998, Wolf 1999, Tomer *et al* 2000).

The optimal velocity model is extended to take into account the vehicle interaction before the next vehicle ahead (the next-nearest-neighbour interaction) (Nagatani 1999a). If the headway Δx_{j+1} of the next vehicle $j+1$ ahead is larger than Δx_j of vehicle j, the driver of vehicle j may wish to proceed with larger velocity than the optimal velocity $V(\Delta x_j)$. The motion equation of the next-nearest-neighbour model is given by

$$\frac{\mathrm{d}^2 x_j(t)}{\mathrm{d}t^2} = \left(\frac{1}{\tau}\right)\left(V(\Delta x_j(t)) + \gamma(V(\Delta x_{j+1}(t) - V(\Delta x_j(t))) - \frac{\mathrm{d}x_j(t)}{\mathrm{d}t}\right). \tag{7}$$

Here, parameter γ represents the strength of the next-nearest-neighbour interaction and $0 \leqslant \gamma \leqslant 1$. The second-term on the right-hand side is the increase of the desired velocity by the next-nearest-neighbour interaction. The next-nearest-neighbour interaction stabilizes the traffic flow and enhances the traffic current.

Mason and Woods (1997) have generalized the model (2) to take into account the two different types of vehicles, say, cars and trucks:

$$\frac{\mathrm{d}^2 x_j(t)}{\mathrm{d}t^2} = \left(\frac{1}{\tau_j}\right)\left(V_j(\Delta x_j(t)) - \frac{\mathrm{d}x_j(t)}{\mathrm{d}t}\right), \tag{8}$$

where τ_j is the delay time of vehicle j, depending on the type of vehicles.

The optimal velocity model is extended to take into account the backward vehicle $j-1$ (Hayakawa and Nakanishi 1998, Nakayama *et al* 2002). A driver looks at the following vehicle $j-1$ as well as the preceding vehicle $j+1$. The motion equation of the backward looking model is given by

$$\frac{\mathrm{d}^2 x_j(t)}{\mathrm{d}t^2} = \left(\frac{1}{\tau}\right)\left(V(\Delta x_j(t)) + V_{\mathrm{B}}(x_j - x_{j-1}) - \frac{\mathrm{d}x_j(t)}{\mathrm{d}t}\right). \tag{9}$$

Here, $V_{\mathrm{B}}(x_j - x_{j-1})$ is the optimal velocity function for backward looking. The backward interaction stabilizes the traffic flow and enhances the traffic current similarly to the next-nearest-neighbour interaction.

Treiber *et al* (1999a, 2000) have presented the IDM to take into account the relative velocity. The model has the following advantage: the vehicle behaves as if accident-free. Lubashevsky *et al* (2002) have proposed the generalization of the optimal velocity model similar to the IDM by the use of a variational principle.

A coupled-map model based on optimal-velocity function is introduced by discretizing the time variable of equation (2) (Yukawa and Kikuchi 1995, Tadaki *et al* 1998).

2.2. Cellular automata

Cellular automata (CA) models have been used for simulating various physical systems because of the simplifications. The simplest traffic model is the CA 184 (Wolfram 1986, 1994, Biham *et al* 1992). The model has been investigated as the totally asymmetric simple exclusion model on one-dimensional lattice for the prototype of interacting systems far from equilibrium (Spohn 1991, Schmittmann and Zia 1998, Schutz 2000). The dynamics is described by

$$x_j(t+1) = x_j(t) + \min[1, x_{j+1}(t) - x_j(t) - 1]. \tag{10}$$

In this model, a particle (vehicle) moves by one lattice spacing if the site ahead is not occupied by other particles. Otherwise, it stops on the site. All particles are updated in parallel (simultaneously). The velocity is either one or zero. Later, Fukui and Ishibashi (1996) have proposed the extended CA model

$$x_j(t+1) = x_j(t) + \min[v_{\max}, x_{j+1}(t) - x_j(t) - 1]. \tag{11}$$

The velocity takes the integer value ranging from 0 to $v_{\max}$. The velocity depends on the headway $\Delta x_j(t)$. If $\Delta x_j(t)$ is larger than maximal velocity $v_{\max}$, the vehicle j moves with the maximal velocity. If $\Delta x_j(t)$ is less than maximal velocity $v_{\max}$, the vehicle moves with velocity $\Delta x_j - 1$. This model is rewritten as

$$x_j(t+1) - 2x_j(t) + x_j(t-1) = \min[v_{\max}, \Delta x_j(t) - 1] - \{x_j(t) - x_j(t-1)\}. \tag{12}$$

By taking a continuous limit $\Delta t \to 0$, one obtains

$$\frac{\mathrm{d}^2 x_j}{\mathrm{d}t^2} = \min[v_{\max}, \Delta x_j(t) - 1] - \frac{\mathrm{d}x_j}{\mathrm{d}t}. \tag{13}$$

The first-term on the right-hand side represents the optimal velocity function. Equation (13) is equivalent to the optimal velocity model (2) with delay time $\tau = 1$ by replacing $V(\Delta x_j(t))$ with $\min[v_{\max}, \Delta x_j(t) - 1]$ (Nishinari and Takahashi 2000, Nishinari 2001). The model (13) has been studied as the piecewise linear optimal velocity model (Nakanishi *et al* 1997).

The extended CA model (12) is a simplified version of the Nagel–Schreckenberg (NaSch) model (Nagel and Schreckenberg 1992, Chowdhury *et al* 2000, Helbing 2001). The NaSch model has been introduced by Nagel and Schreckenberg (1992). The CA model has been recognized as the pioneering work for simulating the real traffic flow. The dynamics is formulated as follows:

$$x_j(t+1) = x_j(t) + \max[0, \min\{v_{\max}, x_{j+1}(t) - x_j(t) - 1, x_j(t) - x_j(t-1) + 1\} - \xi_j(t)], \tag{14}$$

where the Boolean random variable $\xi_j(t) = 1$ with probability p and 0 with probability $1 - p$. The vehicles are updated in parallel according to the four steps: motion, acceleration, deceleration and randomization. The NaSch model has been extended by some researchers (Nagel and Herrmann 1993, Nagel and Paczuski 1995). Schadschneider and Schreckenberg (1993, 1997a) and Schrekenberg *et al* (1995) have presented the mean-field theory for the model (Chowdhury *et al* 2000).

Takayasu and Takayasu (1993) have proposed the CA model of the slow-start rule to take into account the inertia of vehicle. The dynamics is given by

$$x_j(t+1) = x_j(t) + \min[1, x_{j+1}(t) - x_j(t) - 1, x_{j+1}(t-1) - x_j(t-1) - 1]. \tag{15}$$

The motion of vehicle depends not only on the headway at time t but also on the headway at $t - 1$. This model exhibits the metastability. Schadscheider and Schreckenberg (1997b) have also extended the NaSch model to include the slow-start rule. Very recently, Nishinari (2001) has proposed the generalized CA model taking into account the inertia effect and has shown that the model reproduces the real fundamental diagram. Krauss *et al* (1996, 1997, 1998) have developed and have investigated the Gipps model (1981). The model exhibits the three distinct behaviours: the FT, the metastability and the congested traffic.

Helbing and Schreckenberg (1999) have presented the discrete and noisy optimal velocity model to construct a link between the NaSch model and the optimal velocity model. Various CA models have been proposed and investigated (see the paper of Chowdhury *et al* (2000) and references therein). Cheybami *et al* (2000) have studied the effect of the stochastic boundary conditions on the traffic flow in the deterministic NaSch model.

The CA model has been extended to take into account quenched random hopping probabilities of the individual cars (Nagatani 1995, Evans 1996, 1997, Krug and Ferrari 1996, Ktitarev *et al* 1997). It has been found that Bose–Einstein-like condensation occurs for platoon formation.

2.3. Gas-kinetic models

The kinetic theory treats vehicles as a gas of interacting particles. Various versions have been developed to extend and modify the gas-kinetic theory for traffic flow (Prigogine and Herman 1971, Paveri-Fontana 1975, Ben-Naim *et al* 1994, Helbing 1996a, 1997b, Nagatani 1996, 1997a, b, Wagner *et al* 1996, Ben-Naim and Krapivsky 1997, 1998, 1999, Wagner 1997, 1998, Helbing and Treiber 1998a). Prigogine and Herman have proposed the Boltzmann equation for the traffic

$$\frac{\partial f(x,v,t)}{\partial t}+v\frac{\partial f(x,v,t)}{\partial x}=-\frac{f(x,v,t)-\rho(x,t)F_{\rm des}(v)}{\tau_{\rm rel}}+\left(\frac{\partial f(x,v,t)}{\partial t}\right)_{\rm int}, \tag{16}$$

where the first-term on the right-hand side represents the relaxation of the velocity distribution function $f(x,v,t)$ to the desired velocity distribution $\rho(x,t)F_{\rm des}(v)$ with the relaxation time $\tau_{\rm rel}$ in the absence of the interactions of vehicles and the second-term on the right-hand side takes into account the change arising from the interactions among vehicles.

Lehmann (1996) has presented the simplest model which uses the desired velocity distribution determined from the empirical data:

$$\frac{\partial f(x,v,t)}{\partial t}+v\frac{\partial f(x,v,t)}{\partial x}=-\frac{f(x,v,t)-f_{\rm des}(v,\rho)}{\tau_{\rm rel}}. \tag{17}$$

By taking into account the different personalities of drivers, Paveri-Fontana (1975) has proposed the generalized gas-kinetic model:

$$\frac{\partial g(x,v,v_{\rm des},t)}{\partial t}+v\frac{\partial g(x,v,v_{\rm des},t)}{\partial x}+\frac{\partial}{\partial v}\left[\left(\frac{v_{\rm des}-v}{\tau}\right)g(x,v,v_{\rm des},t)\right]=\left(\frac{\partial g(x,v,v_{\rm des},t)}{\partial t}\right)_{\rm int}, \tag{18}$$

$$\left(\frac{\partial g(x,v,v_{\rm des},t)}{\partial t}\right)_{\rm int}=f(x,v,t)\int_v^\infty {\rm d}v'(1-P_{\rm pass})(v'-v)g(x,v',v_{\rm des},t) -g(x,v,v_{\rm des},t)\int_0^v {\rm d}v'(1-P_{\rm pass})(v-v')f(x,v',t), \tag{19}$$

where $f(x,v,t)=\int_0^\infty {\rm d}v_{\rm des}\,g(x,v,v_{\rm des},t)$ and $P_{\rm pass}$ is the probability of passing. The velocity distribution function $g(x,v,v_{\rm des},t)\,{\rm d}x\,{\rm d}v\,{\rm d}v_{\rm des}$ represents the number of vehicles at time t between x and $x+{\rm d}x$, having actual velocity between v and $v+{\rm d}v$ and desired velocity between $v_{\rm des}$ and $v_{\rm des}+{\rm d}v_{\rm des}$. This model accounts for the distribution of desired velocity inherent for the driver-vehicle system, i.e. the difference among the individual vehicles.

By starting with the master equation, Helbing (1997a) has presented the following kinetic equation

$$\frac{\partial f(x,v,t)}{\partial t}+\frac{\partial\,(vf(x,v,t))}{\partial x}+\frac{\partial}{\partial v}\left[\left(\frac{v_{\rm des}-v}{\tau}\right)f(x,v,t)\right]=\frac{1}{2}\frac{\partial^2\,(D_{\rm vf}f(x,v,t))}{\partial v^2}+\left(\frac{\partial f(x,v,t)}{\partial t}\right)_{\rm int}, \tag{20}$$

where $D_{\rm vf}$ is a velocity diffusion constant.

Helbing (1995, 1996a, b, 1997a, 1998a) and coworkers (Helbing and Treiber 1998a, Shversov and Helbing 1999) have derived the macroscopic traffic model from (20). Thus, they have constructed a micro–macro link. Henneke *et al* (2000) have performed the simultaneous micro- and macro-simulation.

Ben-Naim and Krapivsky (1997, 1998, 1999) have studied the power-law platoon formation (bunching of cars) as aggregation phenomena by using the kinetic theory (Ben-Naim *et al* 1994, Ispolatov and Krapivsky 2000).

Mahnke and Pieret (1997) have presented the simple model of master equation approach to the jam growth. The evolution equation of jam size n is given by

$$\frac{\mathrm{d}P(n,t)}{\mathrm{d}t} = W_+(n-1)P(n-1,t) + W_-(n+1)P(n+1,t) - \{W_+(n) + W_-(n)\}P(n,t), \tag{21}$$

where $P(n,t)$ is the probability distribution of jam size n at time t and $W_+(n)$ ($W_-(n)$) is the transition rate from jam size n to $n+1$ ($n-1$).

The kinetic theories of a single-lane highway have been extended to the two-dimensional flow for city traffic and the multi-lane traffic (Nagatani 1996, 1997a, Chowdhury *et al* 2000).

2.4. Macroscopic traffic models

The macroscopic traffic theory treats traffic as an effectively one-dimensional compressible fluid. The traffic states at position x and time t is described in terms of the spatial vehicle density $\rho(x,t)$ and the average velocity $v(x,t)$. Lighthill and Whitham (1955) have proposed the oldest continuum model. The model is described by the continuity equation of fluids

$$\frac{\partial \rho(x,t)}{\partial t} + \frac{\partial q(x,t)}{\partial x} = 0, \tag{22}$$

where $q(x,t) = \rho(x,t)v(x,t)$ is the traffic current (or flow). Lighthill and Whitham assume that the traffic current is determined by the fundamental (flow-density) diagram: $q(x,t) = Q_0(\rho(x,t))$. The nonlinear equation describes the propagation of kinematic waves. To avoid an instability of shock front, a small diffusion term is added

$$q(x,t) = Q_0(\rho(x,t)) - D\frac{\partial \rho(x,t)}{\partial x}. \tag{23}$$

Assuming the simple fundamental diagram $Q_0 = v_{\max}\rho(x,t)\,(1-\rho(x,t))$, the Burgers equation is obtained. Until now, various macroscopic traffic models have been proposed (Payne 1971, 1979, Phillips 1979). Finally, the complete continuum model of the highway traffic flow is given by

$$\frac{\partial \rho}{\partial t} + \frac{\partial(\rho v)}{\partial x} = 0, \tag{24}$$

$$\rho\frac{\partial v}{\partial t} + \rho v\frac{\partial v}{\partial x} = \frac{\rho}{\tau}[V(\rho) - v] - c_0^2\frac{\partial \rho}{\partial x} + \mu\frac{\partial^2 v}{\partial x^2}, \tag{25}$$

where τ, c_0^2 and μ are phenomenological constants. The phenomenological function $V(\rho)$ represents the desired velocity achieved in the steady state. The constant τ is the relaxation time to the steady state. The desired velocity $V(\rho)$ corresponds to the optimal velocity in the microscopic model. The relaxation time τ corresponds to the delay time in the optimal velocity model.

Kerner and Konhauser (1993, 1994) have investigated the continuum model and have shown that the jamming transition occurs at high density and the density waves appear as the

autosolitons. Later, Lee *et al* (1999) have extended the model to take into account the inflow on-ramp. Some attempts have been made for deriving the macroscopic traffic model from the microscopic model. Berg *et al* (2000) have derived the continuum model from the optimal velocity model (2). By using a series expansion of the headway in terms of the density, the following expression is obtained

$$\frac{\partial v}{\partial t}+v\frac{\partial v}{\partial x}=\frac{1}{\tau}\left[V(\rho)-v\right]+\frac{V'(\rho)}{\tau}\left[\frac{1}{2\rho}\frac{\partial \rho}{\partial x}+\frac{1}{6\rho^2}\frac{\partial^2\rho}{\partial x^2}-\frac{1}{2\rho^3}\left(\frac{\partial \rho}{\partial x}\right)^2\right]. \tag{26}$$

Equation (26) is analogous to the Kerner–Konhausser model (25). However, an important difference between (25) and (26) lies in the coefficients. The coefficients of (25) are the phenomenological parameters, while the coefficients of (26) depend on the parameters of the microscopic model. It is easy to identify the parameters of (26) though it is difficult to determine the phenomenological constants τ, c_0^2 and μ in (25).

Nelson (2000) has derived the modified Lighthill–Whitham model by the use of the different method. He assumes that drivers compensate for the delay τ by adjusting to the density seen at some anticipation distance L_a ahead of their current position. The actual speed at position x and time t is given by

$$v(x,t)=V(\rho(x+L_a-V\tau,t-\tau)), \tag{27}$$

where $V(\rho)$ is the desired velocity at density ρ. By expanding the right-hand side to first order of τ and L_a, the following expression of traffic current is obtained instead of (23)

$$\begin{aligned}q(x,t)&=\rho(x,t)v(x,t)\\&=Q_0(\rho(x,t))+\rho(x,t)[L_aV'(\rho(x,t))+\tau\rho(x,t)\{V'(\rho(x,t))\}^2]\frac{\partial\rho}{\partial x}.\end{aligned} \tag{28}$$

It is easy to identify the parameters τ and L_a since the model is connected to the microscopic model (1).

A lattice hydrodynamic model has been proposed to have the same mathematical properties as the optimal velocity model (Nagatani 1999b, c). The model has been extended to the two-dimensional lattice for the city traffic. Two types of vehicles are considered: the first type moves only to the positive x-direction and the second type only to the positive y-direction. The continuity equations of x and y vehicles are given by

$$\frac{\partial\rho_x(x,y,t)}{\partial t}+\frac{\partial\rho_x(x,y,t)u(x,y,t)}{\partial x}=0, \tag{29}$$

$$\frac{\partial\rho_y(x,y,t)}{\partial t}+\frac{\partial\rho_y(x,y,t)v(x,y,t)}{\partial y}=0, \tag{30}$$

where $\rho_x(x,y,t)$ and $\rho_y(x,y,t)$ are the local densities of x and y vehicles at position (x,y) at time t and $u(x,y,t)$ and $v(x,y,t)$ are the local speeds of x and y vehicles at position (x,y) at time t. The traffic currents of x and y vehicles are given by

$$\rho_x(x,y,t)u(x,y,t)=\rho_{x,0}V(\rho(x+L_a,y,t-\tau)), \tag{31}$$

$$\rho_y(x,y,t)u(x,y,t)=\rho_{y,0}V(\rho(x,y+L_a,t-\tau)), \tag{32}$$

where $\rho(x,y,t)$ $(=\rho_x(x,y,t)+\rho_y(x,y,t))$ is the local total density at position (x,y) at time t and $\rho_{x,0}$ and $\rho_{y,0}$ are the average densities of x and y vehicles. By making the transformation from the derivatives to the differences, one obtains the two-dimensional lattice hydrodynamic model:

$$\rho_x(m,n,t+2\tau)-\rho_x(m,n,t+\tau)+\tau\rho_0\rho_{x,0}[V(\rho(m+1,n,t))-V(\rho(m,n,t))]=0, \tag{33}$$

$$\rho_y(m,n,t+2\tau)-\rho_y(m,n,t+\tau)+\tau\rho_0\rho_{y,0}[V(\rho(m,n+1,t))-V(\rho(m,n,t))]=0, \tag{34}$$

where site (m,n) indicates the position on the square lattice and $L_a=1/\rho_0$. The two-dimensional lattice model is an extended version of equation (4).

2.5. Micro–macro link

The macroscopic traffic models have been derived from the gas kinetic models (Helbing 1996b,1998c, Wagner 1997, Treiber *et al* 1999, Klar and Wegener 1999a, b). Very recently, Lee *et al* (2001) have addressed the relationship between microscopic car-following models and macroscopic traffic models. The derivation from the optimal velocity model (2) to the hydrodynamic model (25) is given here. We follow the procedure by Lee *et al* (2001). Two microscopic field variables are introduced: density field $\hat{\rho}(x,t) = \sum_j \delta(y_j(t) - x)$ and current (flow) field $\hat{q}(x,t) = \sum_j \dot{y}_j(t)\delta(y_j(t) - x)$ where $y_j(t)$ is the coordinate of the jth vehicle at time t. The coarse-grained density $\rho(x,t)$ and current $q(x,t)$ are defined as

$$\begin{aligned} \rho(x,t) &\equiv \int \mathrm{d}x'\mathrm{d}t'\, \phi(x-x', t-t')\hat{\rho}(x',t'), \\ q(x,t) &\equiv \int \mathrm{d}x'\mathrm{d}t'\, \phi(x-x', t-t')\hat{q}(x',t'), \end{aligned} \tag{35}$$

where coarse-graining envelope function $\phi(x,t)$ is non-negative valued and normalized. By integrating parts and changing variables, one obtains the continuity equation:

$$\frac{\partial \rho(x,t)}{\partial t} + \frac{\partial q(x,t)}{\partial x} = 0. \tag{36}$$

After some algebra, one obtains the dynamic equation for $q(x,t)$

$$\frac{\partial q(x,t)}{\partial t} = \rho(x,t)\left\langle \ddot{y}_j(t')\right\rangle_{(x,t)} - \frac{\partial}{\partial x}\left[\rho(x,t)\left\langle \dot{y}_j^2(t')\right\rangle_{(x,t)}\right], \tag{37}$$

where the bracketed average is defined as

$$\left\langle \ddot{y}_j(t')\right\rangle_{(x,t)} \equiv \frac{1}{\rho(x,t)} \int \mathrm{d}x'\mathrm{d}t'\, \phi(x-x', t-t') \sum_j \ddot{y}_j(t')\delta(y_j(t') - x').$$

The macroscopic velocity field $v(x,t)$ is introduced as $v(x,t) \equiv \langle \dot{y}_j(x',t')\rangle_{(x,t)} = q(x,t)/\rho(x,t)$. Equation (37) is rewritten in terms of ρ and v as follows:

$$\rho\left(\frac{\partial v}{\partial t} + v\frac{\partial v}{\partial x}\right) = \rho\left\langle \ddot{y}_j(t')\right\rangle_{(x,t)} - \frac{\partial \rho\theta}{\partial x}, \tag{38}$$

where $\theta(x,t) \equiv \langle \dot{y}_j^2(t')\rangle_{(x,t)} - v(x,t)^2$. The bracketed average is derived by coarse-graining of the optimal velocity model (2):

$$\langle \ddot{y}_j\rangle = \left(\frac{1}{\tau}\right)[\langle V(\Delta y_j)\rangle - v]. \tag{39}$$

The expansion of the coarse-grained optimal velocity with $\langle \Delta y_j\rangle$ leads to

$$\langle V(\Delta y_j)\rangle = V(\langle \Delta y_j\rangle) + \sum_{m=2}^{\infty} \frac{1}{m!} V^{(m)}(\langle \Delta y_j\rangle)\langle(\Delta y_j - \langle \Delta y_j\rangle)^m\rangle. \tag{40}$$

The coarse-grained headway is expressed in terms of density:

$$\langle \Delta y_j\rangle = \rho^{-1} + \frac{1}{2\rho}\frac{\partial \rho^{-1}}{\partial x} + \frac{1}{6\rho^2}\frac{\partial^2 \rho^{-1}}{\partial x^2}. \tag{41}$$

Thus, the leading term of (40) is expanded as

$$V(\langle \Delta y_j\rangle) = V(\rho^{-1}) + \frac{V'(\rho^{-1})}{2\rho}\frac{\partial \rho^{-1}}{\partial x} + \frac{1}{6\rho^2}\frac{\partial^2 v}{\partial x^2}. \tag{42}$$

Finally, the momentum equation is obtained

$$\frac{\partial v}{\partial t} + v\frac{\partial v}{\partial x} = \left(\frac{1}{\tau}\right)[V(\rho^{-1}) - v] - \frac{V'}{2\tau\rho^3}\frac{\partial \rho}{\partial x} + \frac{1}{6\tau\rho^2}\frac{\partial^2 v}{\partial x^2}. \tag{43}$$

The momentum equation has a structure similar to the macroscopic model (25) used by Kerner and Kohnhauser (1993) and Lee *et al* (1998, 1999). The phenomenological constants of (25) are determined from the microscopic car-following model (2).

3. Instability and phase transition

3.1. Linear stability analysis

In the optimal velocity models, all the vehicles move with the same headway h and the optimal velocity $V(h)$ at a low density of vehicles. When the density is higher than the critical value, the traffic jam appears as density waves propagating backward. We consider the stability of the uniform traffic flow. The uniform traffic flow is defined by such a state that all vehicles move with constant headway h and the optimal velocity $V(h)$. The uniform traffic flow is a solution of the optimal velocity model. The solution is given by

$$x_{j,0}(t) = hj + V(h)t \qquad \text{with } h = \frac{L}{N}, \tag{44}$$

where N is the number of vehicles, L is the road length and density ρ is $1/(h+1)$.

We apply the linear stability theory to the optimal velocity model (1). By adding a small fluctuation to the steady-state solution, one can study whether or not fluctuations amplify. If fluctuations added to the steady-state solution decay in time, the steady state is stable. Otherwise, fluctuations amplify in time and the uniform traffic flow changes the different dynamical state. Let $y_j(t)$ be a small deviation from the uniform solution $x_{j,0}(t)$: $x_j(t) = x_{j,0}(t) + y_j(t)$. Then, the linear equation is obtained from equation (1)

$$\frac{\mathrm{d}y_j(t+\tau)}{\mathrm{d}t} = V'(h)\Delta y_j(t), \tag{45}$$

where $V'(h)$ is the derivative of optimal velocity $V(\Delta x)$ at $\Delta x = h$. By expanding $y_j(t) = Y\exp(ikj + zt)$, one obtains

$$z\mathrm{e}^{z\tau} = V'(h)(\mathrm{e}^{ik} - 1). \tag{46}$$

By solving equation (46) with z, one finds that the leading term of z is order of ik. When $ik \to 0$, $z \to 0$. Let us derive the long wave expansion of z, which is determined order by order around $ik \approx 0$. By expanding $z = z_1(ik) + z_2(ik)^2 + \cdots$, the first- and second-order terms of ik are obtained

$$z_1 = V'(h) \qquad \text{and} \qquad z_2 = -\tfrac{1}{2}V'(h)(2V'(h)\tau - 1). \tag{47}$$

If z_2 is a negative value, the uniform flow becomes unstable for long wavelength modes. When z_2 is a positive value, the uniform flow is stable. The neutral stability condition is given by $z_2 = 0$:

$$\tau = \frac{1}{2V'(h)}. \tag{48}$$

For small disturbances of long wavelengths, the uniform traffic flow is unstable if delay τ is larger than $1/2V'(h)$: $\tau > 1/2V'(h)$. Otherwise, it is stable. Figure 2 shows the region map in parameter space $(h, 1/\tau)$ for $x_c = 5$ and $v_{max} = 2.0$. The solid curve indicates the neutral stability line. In the region above the neutral stability line, the traffic flow with the uniform headway and velocity profiles is stable. In the region below the neutral stability line, the traffic flow becomes unstable. One finds that there is a critical point at $h(=\Delta x) = x_c$ and $\tau = \tau_c = 1/v_{max}$. Therefore, if $\tau < \tau_c$, the uniform flow is always stable irrespective of density (headway).

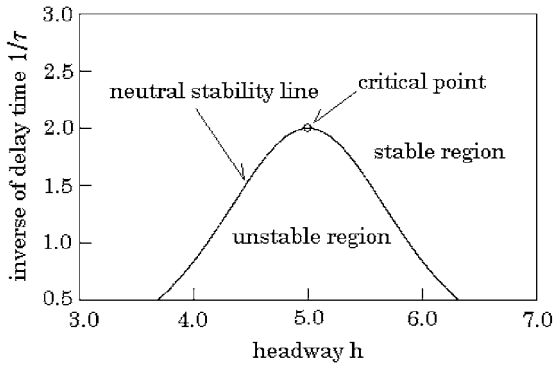

Figure 2. Region map in parameter space $(h, 1/\tau)$ for $x_c = 5$ and $v_{max} = 2.0$. The solid curve indicates the neutral stability line. In the region above the neutral stability line, the traffic flow with the uniform headway and velocity profiles is stable. In the region below the neutral stability line, the traffic flow becomes unstable.

The neutral stability condition of differential equation model (2) is also obtained and is consistent with equation (48) (Bando *et al* 1995). The neutral stability condition of difference equation model (3) is given by $\tau = 1/3V'(h)$ and is different from equation (48) (Nagatani *et al* 1998, Nagatani 1999a). The neutral stability line agrees with the jamming transition curve obtained from simulation. The neutral stability curves are obtained for the next-nearest-neighbour interaction model (7) and the backward looking model (9). The linear stability conditions for models (1), (2), (3), (7) and (9) are summarized as follow:

$$\begin{aligned}
&\tau < \frac{1}{2V'(h)} && \text{for equations (1) and (2),}\\
&\tau < \frac{1}{3V'(h)} && \text{for equation (3),}\\
&\tau < \frac{1+2\gamma}{2V'(h)} && \text{for equation (7),}\\
&\tau < \frac{V'(h) - V'_{\mathrm{B}}(h)}{2[V'(h) + V'_{\mathrm{B}}(h)]^2} && \text{for equation (9).}
\end{aligned} \tag{49}$$

The linear stability analysis has been applied to the macroscopic traffic models. The neutral stability conditions have been derived. Kerner and Konhauser (1993) and Kurtze and Hong (1995) have derived the linear stability condition for the fluid dynamic model of traffic described by equations (24) and (25). Equations (24) and (25) admit a simple steady-state solution representing uniform flow: $\rho(x,t) = \rho_0$, $v(x,t) = V(\rho_0) \equiv v_0$. By assuming that traffic is initially in a state which differs infinitesimally from the uniform flow, one decomposes this flow into

$$\begin{aligned}
\rho(x,t) &= \rho_0 + \sum_k \delta\rho_k \exp(\mathrm{i}kx + \sigma_k t),\\
v(x,t) &= v_0 + \sum_k \delta v_k \exp(\mathrm{i}kx + \sigma_k t).
\end{aligned} \tag{50}$$

By substituting the expressions into (24) and (25) and linearizing in $\delta\rho_k$ and δv_k, one obtains the linear equations. One finds that each linear growth rate σ_k must satisfy the quadratic equation

$$(\sigma_k + \mathrm{i}v_0 k)^2 + \left[\frac{1}{\tau} + \mu k^2\right](\sigma_k + \mathrm{i}v_0 k) + c_0^2 k^2 + \mathrm{i}\frac{\rho_0 V'(\rho_0)}{\tau}k = 0, \tag{51}$$

where the prime represents derivative with respect to ρ_0. If both roots of this quadratic have negative real parts, the uniform traffic flow is stable against all infinitesimal perturbations. The linear stability condition is given by

$$\rho_0 V'(\rho_0)^2 < c_0^2 \rho_0^{-1}. \tag{52}$$

This linear stability condition for the macroscopic model (24) and (25) is compared with (48) and (49) for the optimal velocity models.

If one uses the expression $c_0^2 = V'(\rho_0^{-1})/2\tau\rho_0^2$ in (43) derived by Lee *et al* (2001), the following linear stability condition is obtained

$$\tau < \frac{1}{2V'(\rho_0^{-1})}, \tag{53}$$

where the prime represents derivative with respect to ρ_0^{-1}. Thus, the macroscopic linear stability condition (53) agrees with the microscopic stability condition (49).

3.2. From instability to density waves

When small noises are added to the uniform traffic flow, its flow is stable and robust for low density because the stability condition (49) is satisfied. When the density is higher than the critical density, the condition (49) is not satisfied. Then, the uniform flow including noises is unstable, the noises amplify in time and the uniform flow changes finally to the inhomogeneous traffic flow with propagating density waves. Figure 3 shows the typical profile of the inhomogeneous flow obtained from simulation of (3) where $v_{\max} = 2.0$, $\tau = 0.5$, $x_c = 5.0$ and average headway $\Delta x_0 = 5.0$. The pattern (*a*) indicates the time evolution of the headway profile in the unstable region in figure 2. The headway profile (*b*) is obtained after sufficiently large time. The initial uniform flow evolves in time to the inhomogeneous flow with the kink density waves. The density wave propagates backward with constant speed. The density wave is robust and keeps the kink form. The high-density region is the jammed state of vehicles and the low-density region is the FT state. Thus, the coexisting phase of both jammed and free states appears in the unstable region of figure 2.

The upper dotted line of headway profile (*b*) indicates the value of headway outside the jammed state. The bottom dotted line indicates the value of headway within the jam. These values keep constant values for constant τ and depend only on τ. By considering long-time evolution, only two distinct headways survive for the coexisting phase. Figure 4 shows the plot of the headways within and outside the jam for various values of τ. The solid curve connecting their circles gives the coexisting curve in the phase space $(h, 1/\tau)$. The dotted line indicates the neutral stability curve.

Figure 5 shows the plot of the traffic current q against density $\rho = 1/(h + 1)$ where $v_{\max} = 2.0$, $\tau = 0.5$ and $x_c = 5.0$. The traffic current increases with density in the low-density

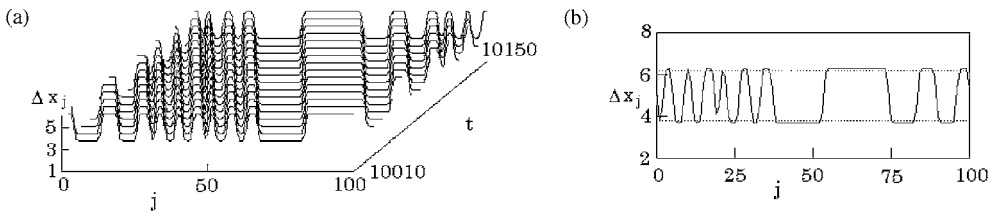

Figure 3. Typical profile of the inhomogeneous flow obtained from simulation of (3). (*a*) Time evolution of the headway profile in the unstable region in figure 2. (*b*) Headway profile at $t = 10\,100$.

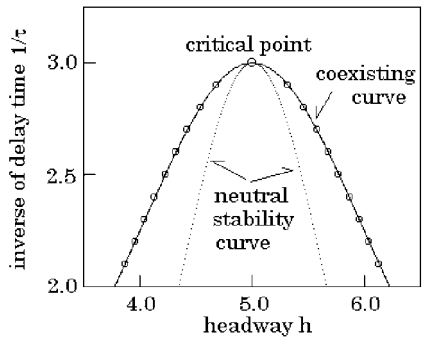

Figure 4. Plot of the headways within and outside the jam for various values of τ. The solid curve connecting their circles gives the coexisting curve in the phase space $(h, 1/\tau)$. The dotted line indicates the neutral stability curve. This presents the phase diagram.

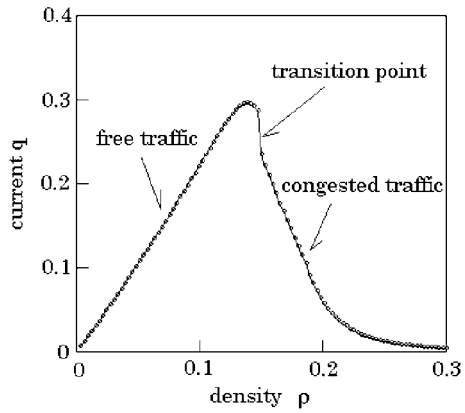

Figure 5. Plot of the traffic current q against density $\rho = 1/(h+1)$.

region, reaches the maximal value, decreases discontinuously at the gap and then decreases continuously with increasing density. The critical density at the gap agrees with the jamming transition point: the neutral stability point.

The dependency of jamming transition on the strength of noises (fluctuations) has been studied for the moving group of many vehicles (Nagatani 2000a). The traffic flow on a single-lane highway is a unidirectionally interacting many particle system since a vehicle interacts with one vehicle ahead. When a downstream vehicle changes the speed or headway, the variation propagates upstream. Then, it will die out or evolve to the density waves. Without fluctuation (noise), the traffic flow is uniform and homogeneous under open boundary condition. However, when the velocity of a leading vehicle fluctuates at a finite amplitude, the density waves may propagate upstream and the formation of the density waves depends on the headway between vehicles (or velocity) and the amplitude of fluctuation. Figure 6 shows the spatio-temporal evolution of headway against the vehicle number j in the difference equation model (3). When the traffic state is in the linear stable region, the traffic flow remains uniform and homogeneous for an infinitesimal fluctuation. If the traffic state is in the unstable region, the homogeneous traffic flow breaks down and the density waves appear (see the patterns (a) and (b) in figure 6). The pattern (a) exhibits the moving localized cluster (MLC) of jams. The MLC appears just near the transition point. It is produced periodically. The pattern (b) exhibits the oscillating

congested traffic (OCT). The number of density waves increases accordingly as the headway approaches to the turning point x_c of the optimal velocity function (6).

Figure 7 shows the phase diagram of different kinds of traffic triggered by fluctuations in (v_b, δ) space where v_b is the velocity of leading vehicle and δ is the amplitude of fluctuations.

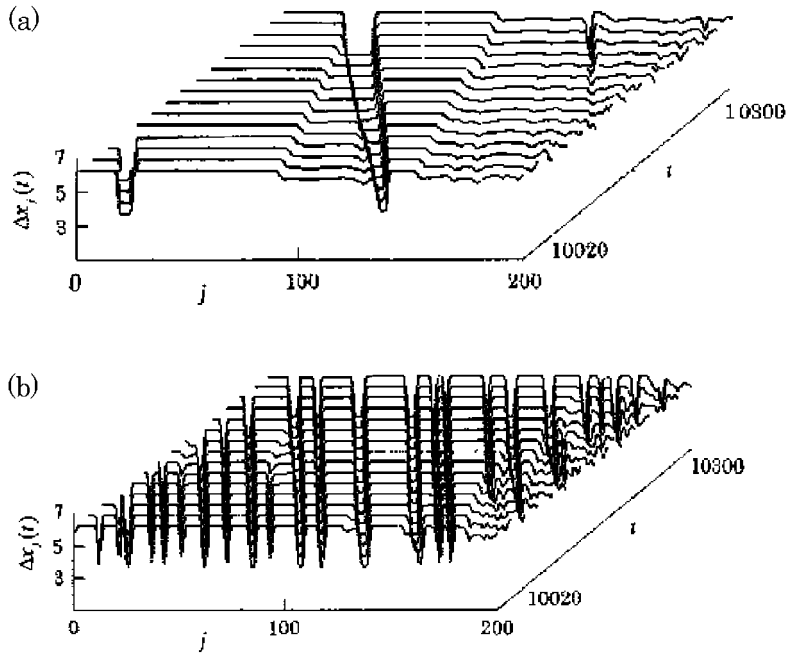

Figure 6. Spatio-temporal evolution of headway for 200 vehicles moving with a group. (*a*) Pattern for the MLC of jams just near the transition point. (*b*) Pattern of the OCT in an unstable region.

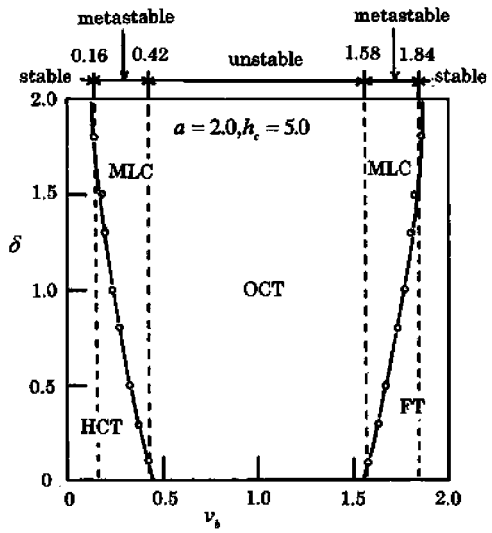

Figure 7. Phase diagram of different kinds of traffic triggered by fluctuations in (v_b, δ) space where v_b is the velocity of leading vehicle and δ is the amplitude of fluctuations. Displayed are the FT, the MLCs, the OCT and the HCT.

The circular points indicate the transition points between the stable and unstable regions. The dotted lines of $v_b = 0.42$ and $v_b = 1.58$ represent the neutral stability lines. The dotted lines of $v_b = 0.16$ and $v_b = 1.84$ represent the velocities of the coexisting lines for $a = 1/\tau = 2.0$ and $x_c = 5.0$. For an infinitesimal fluctuation $\delta \to 0$, the transition points are consistent with the neutral stability points. With increasing the amplitude of fluctuations, the transition points approach to the coexisting line. The MLCs occur just near the transition point. Within the transition points, the OCT occurs. Thus, the jamming transition depends on both velocity and strength of fluctuation.

3.3. Ginzburg–Landau equation and phase diagram

The jamming transition has properties very similar to the conventional phase transition even if the traffic system is far from equilibrium. With increasing density, the FT flow changes to the jammed traffic at a specific value of density. The high-density traffic flow results in the formation of traffic jams in which the FT of low density coexists with the jammed traffic of high density. The FT and jammed traffic correspond respectively to the gas and liquid phases in the conventional gas–liquid phase transition: the headway or vehicle density correspond to the volume or density and the inverse $1/\tau$of the delay time (sensitivity a) corresponds to temperature. Figure 4 exhibits the similarity to the phase diagram of gas–liquid phase transition. The coexisting curve represents the phase separation line. The neutral stability line represents the spinodal line. The region between the coexisting curve and the neutral stability line corresponds to the metastable region. The metastability has been observed as the hystereris phenomenon appearing near the point of maximal current in the fundamental diagram (Barovic *et al* 1998, Krauss 1998, Helbing 2001). The metastability is characteristic of the first-order phase transition. Also, the critical point corresponds to that of the gas–liquid phase transition.

The small parameter ε representing the neighbourhood of the critical point is defined as $\tau/\tau_c = 1 + \varepsilon^2$. By sustaining the perturbed terms less than sixth-order term of ε (Cross and Hohenberg 1993), one obtains the TDGL equation (Kawasaki 1984, Nagatani 1998) from model (1):

$$\frac{\partial S}{\partial t} = -\left(\frac{\partial}{\partial X} - \frac{1}{2}\frac{\partial^2}{\partial X^2}\right)\frac{\delta \Phi(S)}{\delta S} \tag{54}$$

with $X = j + \{2V'(x_c)^2\tau\}t$ and $S(X, t) = \Delta x_j(t) - x_c$,

$$\Phi(S) = \int \mathrm{d}x \left(\frac{V'(x_c)}{48}\left(\frac{\partial S}{\partial X}\right)^2 + \phi(S)\right),$$

and the *thermodynamic potential*

$$\phi(S) = -V'(x_c)\left(\tau V'(x_c) - \frac{1}{2}\right)S^2 + \frac{|V'''(x_c)|}{24}S^4. \tag{55}$$

The thermodynamic potential (55) has the double wells, two minimums below the critical point ($1/\tau < 1/\tau_c\ (= 2V'(x_c))$). The TDGL equation (54) has two steady-state solutions except for a trivial solution $S = 0$: the one is the uniform solution

$$S(X, t) = \pm\left[\frac{6V'(x_c)(2V'(x_c)\tau - 1)}{|V'''(x_c)|}\right]^{1/2}, \tag{56}$$

and the other is the kink solution

$$S(X, t) = \pm\left[\frac{6V'(x_c)(2V'(x_c)\tau - 1)}{|V'''(x_c)|}\right]^{1/2} \tanh[\{12(2V'(x_c)\tau - 1)\}^{1/2}(X - X_0)], \tag{57}$$

where X_0 is a constant.

The coexisting curve, the spinodal line and the critical point can be obtained from thermodynamic potential (55) similarly to the conventional thermodynamic potential of phase transition (Stanley 1971). The coexisting curve is given by the condition

$$\frac{\partial \phi}{\partial S} = 0 \qquad \text{and} \qquad \frac{\partial^2 \phi}{\partial S^2} > 0. \tag{58}$$

One obtains the coexisting curve in terms of the original parameters

$$(\Delta x)_{\mathrm{co}} = x_{\mathrm{c}} \pm \left[\frac{6V'(x_{\mathrm{c}})(2V'(x_{\mathrm{c}})\tau - 1)}{|V'''(x_{\mathrm{c}})|} \right]^{1/2}. \tag{59}$$

The spinodal line is given by the condition

$$\frac{\partial^2 \phi}{\partial S^2} = 0. \tag{60}$$

One obtains the spinodal line

$$(\Delta x)_{\mathrm{co}} = x_{\mathrm{c}} \pm \left[\frac{2V'(x_{\mathrm{c}})(2V'(x_{\mathrm{c}})\tau - 1)}{|V'''(x_{\mathrm{c}})|} \right]^{1/2}. \tag{61}$$

By expanding the neutral stability condition (48) around the critical point $V'(x_{\mathrm{c}})$: $V'(\Delta x) = V'(x_{\mathrm{c}}) + V'''(x_{\mathrm{c}})(\Delta x - x_{\mathrm{c}})^2/2$, one obtains the spinodal line (61). Thus, the spinodal line is consistent with the neutral stability line around the critical point. Indeed, the coexisting curve (59) and the spinodal line (61) agree with those obtained from simulation for $1/\tau > V'(x_{\mathrm{c}})$ though equations (59) and (61) are derived by the perturbation around the critical point. The critical point is given by the condition

$$\frac{\partial \phi}{\partial S} = 0 \qquad \text{and} \qquad \frac{\partial^2 \phi}{\partial S^2} = 0. \tag{62}$$

One obtains the critical point

$$(\Delta x)_{\mathrm{c}} = x_{\mathrm{c}} \qquad \text{and} \qquad \frac{1}{\tau_{\mathrm{c}}} = 2V'(x_{\mathrm{c}}). \tag{63}$$

This is consistent exactly with the critical point obtained from the neutral stability condition (48). Thus, the thermodynamic theory for the jamming transition is formulated in terms of the TDGL equation.

3.4. Traffic states in the presence of inhomogeneities

The jamming transition between the free flow and the jammed state has been studied without any inhomogeneity on highway. When vehicles pass ramps or other spatial inhomogeneities of a freeway, the different kinds of congested traffic are triggered by the inhomogeneities. The inhomogeneities affect the traffic flow as the bottlenecks. Lee *et al* (1999) have investigated the traffic states induced by an on-ramp inflow with the use of macroscopic traffic model. By varying the inflow, traffic flow breaks down to the distinct dynamic states. They have derived the phase diagram for the different traffic states: the pinned localized cluster (PLC), the recurring hump state, the triggered stop-and-go (TSG) traffic and the OCT. Helbing *et al* (1999) have presented a phase diagram of the different kinds of congested traffic in the presence of on-ramp inflow by using the nonlocal, gas-kinetic-based traffic model. Nagatani (2000b) has studied the phase diagram of noisy traffic states in the presence of a bottleneck by the use of the optimal velocity model.

Very recently, Treiber *et al* (2000) have investigated the spatio-temporal structure of distinct states for traffic near on-ramps by the use of the microscopic model (IDM). They have

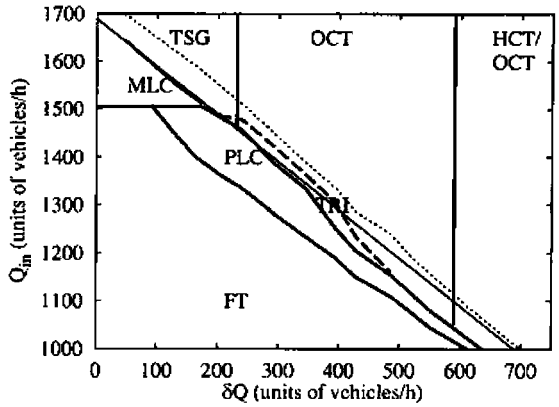

Figure 8. Phase diagram resulting from IDM simulations of an open system with a flow-conserving bottleneck (Treiber *et al* 2000). The control parameters are the traffic current Q_{in} and the bottleneck strength δQ. The distinct traffic states (HCT, OCT, TSG, PLC) are indicated. The MLC indicates the moving localized cluster.

found four distinct congested traffic states: (a) homogeneous congested traffic (HCT), (b) OCT, (c) TSG waves and (d) PLC. The HCT state is the homogeneous congested state with high density extended behind on-ramp. The OCT state consists of many density waves propagating backward from on-ramp. The density profile oscillates in both space and time. In the TSG state, the stop-and-go wave is produced with a constant period. The PLC state consists of high-density region localized just behind on-ramp.

Figure 8 shows the phase diagram resulting from IDM simulations of an open system with a flow-conserving bottleneck. The control parameters are the traffic current Q_{in} and the bottleneck strength δQ. At low traffic current, the FT evolves to the PLC, through the OCT and finally to the HCT with increasing bottleneck strength. For low bottleneck strength, the FT evolves through the MLC to the TSG waves with increasing traffic current. Thus, the inhomogeneities on freeway produce the complex traffic jams. Their density waves have been observed in real traffic (Treiber *et al* 2000). The comparison with the empirical data is given in section 5.

4. Density waves and nonlinear equations

Until now, various density waves have been observed in the traffic flow. The traffic jams have been treated frequently as the density waves. The nonlinear wave equations have been proposed to describe the jams. The Burgers, KdV and MKdV equations have been presented as the typical ones. The proposed wave equations have depended strongly on the traffic models (Newell 1961, Musha and Higuchi 1976, 1978, Whitham 1990, Kerner and Konhauser 1993, Komatsu and Sasa 1995, Kurtze and Hong 1995). Recently, the three distinct nonlinear wave equations have been derived from the optimal velocity model (1) in the unified way (Muramatsu and Nagatani 1999, Nagatani 2000c). The different wave equations describe the density waves appearing in the three distinct regions: the stable traffic region out of the coexisting curve, the metastability region between the coexisting and spinodal lines, and the unstable region within the coexisting curve.

4.1. Burgers equation

In the stable traffic region out of the coexisting curve, the headway (or velocity) profile with any forms at an initial stage evolves in time to the uniform distribution with the same spacing

(velocity) for all vehicles. At an asymptotic stage of the evolving process, a triangular shock wave is observed in the simulation of optimal velocity model (1). Figure 9 shows the relaxation process of the nonuniform flow to the uniform steady flow. The pattern (*a*) shows the time evolution of the headway profile when the initial density profile has the kink–antikink form. At the intermediate stage, the kink density wave evolves to the triangular shock wave. The headway profile (*b*) at $t = 10\,000$ exhibits the triangular shock wave where points *c* and *d* indicate the positions of the shock front and the intersection of the slope. The triangular shock wave propagates backward with a constant speed. The propagation speed is obtained as $V'(\Delta x_0)$ where Δx_0 is the average value of headways.

Let us derive the triangular shock solution from the optimal velocity model (1). By defining the slow variables $X = \varepsilon(j + V'(\Delta x_0)t)$ and $T = \varepsilon^2 t$, setting $\Delta x_j(t) = \Delta x_0 + \varepsilon R(X, T)$ $(0 < \varepsilon \ll 1)$ and expanding equation (1) to the third order of ε, one obtains the nonlinear equation:

$$\frac{\partial R}{\partial T} - V''(\Delta x_0) R \frac{\partial R}{\partial X} = \left(\frac{V'(\Delta x_0)}{2} - V'(\Delta x_0)^2 \tau \right) \frac{\partial^2 R}{\partial X^2}, \tag{64}$$

where $V''(\Delta x_0)$ is negative for $\Delta x_0 > x_c$. Since the coefficient $(V'/2 - V'^2\tau)$ of the second derivative has a positive value in the stable traffic flow satisfying the stability condition (49), equation (64) is just the Burgers equation. The solution for the asymptotic stage $(T \gg 1)$ is a

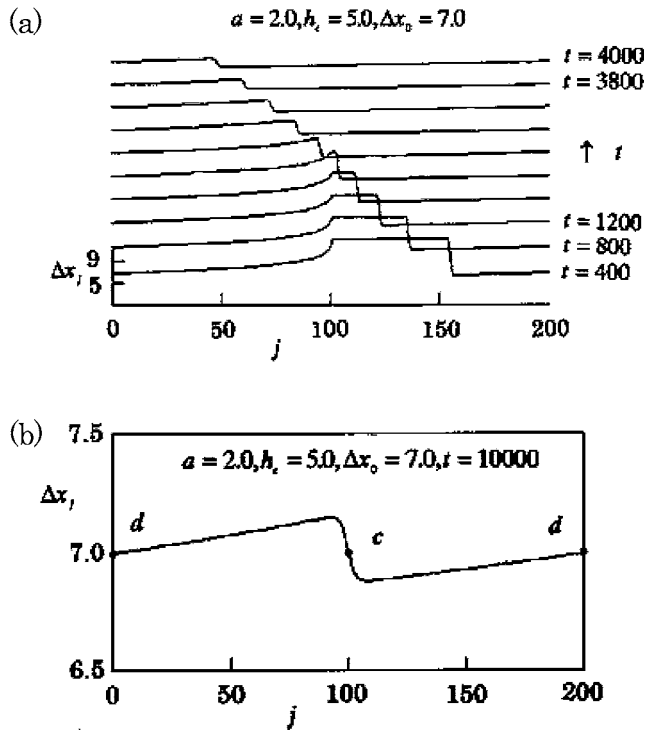

Figure 9. Relaxation process of the nonuniform flow to the uniform steady flow in the stable traffic region above the coexisting curve. (*a*) Time evolution of the headway profile when the initial density profile has the kink–antikink form. (*b*) Headway profile at $t = 10\,000$.

train of N-triangular shock waves (Tatsumi and Kida 1972)

$$R(X,T) = \frac{1}{|V''|T}\left(X - \frac{1}{2}(\eta_m + \eta_{m+1})\right) - \frac{1}{2|V''|T}(\eta_{m+1} - \eta_m)\tanh\left[\frac{C}{4|V''|T}(\eta_{m+1} - \eta_m)(X - \xi_m)\right], \tag{65}$$

where $C = V'/2 - V'^2\tau$, the coordinates of the shock fronts are given by ξ_m ($m = 1, 2, \ldots, N$) and those of the intersections of the slopes with x-axis are given by η_m. The triangular shock wave propagates backward with propagation speed $V'(\Delta x_0)$. The theoretical result agrees with the simulation result. The two slopes at the shock front and intersection scale as t^{-1} and t^{-2}. These results are consistent with the simulation result (Nagatani 2000c).

4.2. KdV equation

Newell (1961) and Whitham (1990) have derived the KdV equation for the optimal velocity model by the use of the following optimal velocity function different from equation (6):

$$V(\Delta x_j(t)) = v_{\max}\{1 - \exp[-\gamma(\Delta x_j(t) - L]\}, \tag{66}$$

where $v_{\max}$ is the maximal velocity, L is the car length and γ is a constant. The *soliton* solution has been obtained from the theoretical analysis. However, such a density wave as the soliton is not obtained from the simulation of optimal velocity model (1) with (66).

Later, Kurtze and Hong (1995) have derived the KdV equation from the hydrodynamic model by the use of the nonlinear analysis method. They have conjectured that the single-pulse density wave obtained from the simulation is the soliton. However, the single-pulse density wave of the simulation is not the soliton but the kink–antikink density wave (Kerner and Konhauser 1993, Kerner *et al* 1995, Muramatsu and Nagatani 1999). Muramatsu and Nagatani (1999) have shown that the soliton density wave appears only just above the neutral stability line (spinodal line) by the use of the nonlinear analysis and simulation for the optimal velocity model (2) with (6). The soliton occurs only in the metastable region just above the spinodal line.

Let us derive the KdV equation from (2) with (6). Suppose that the headway of uniform traffic flow is near the neutral stability point. One quantifies this by writing

$$1 - \frac{a_s}{a} = \varepsilon^2 \qquad (0 < \varepsilon \ll 1), \tag{67}$$

where $a_s = 2V'(\Delta x_0)$ and a_s ($=1/\tau_s$) is the sensitivity at the neutral stability point. We consider the slowly varying behaviour at long wavelengths near the neutral stability line. One extracts slow scales for space variable j and time variable t. One defines the slow variables X and T: $X = \varepsilon(j + V'(\Delta x_0)t)$ and $T = \varepsilon^3 t$. By setting the headway as $\Delta x_j(t) = \Delta x_0 + \varepsilon^2 R(X,T)$ and expanding to the sixth order of ε, one obtains

$$\varepsilon^5 a\left[\frac{\partial R}{\partial T} - \frac{V'(\Delta x_0)}{6}\frac{\partial^3 R}{\partial X^3} - V''(\Delta x_0)R\frac{\partial R}{\partial X}\right] + \mathrm{O}(\varepsilon^6) = 0. \tag{68}$$

If one ignores the $\mathrm{O}(\varepsilon^6)$ terms, equation (68) is just the KdV equation with a soliton solution as the desired solution. The amplitude of soliton solutions of the KdV equation is a free parameter. The perturbation term $\mathrm{O}(\varepsilon^6)$ of perturbed KdV equation (68) selects a unique member of the continuous family of KdV solitons. By satisfying the solvability condition, one obtains the soliton solution

$$\Delta x_j(t) = \Delta x_0 + \frac{14V'(\Delta x_0)}{3V''(\Delta x_0)}\left|\frac{a_s}{a} - 1\right| \times \sec h^2\left[\sqrt{\frac{7}{3}\left|\frac{a_s}{a} - 1\right|}\left\{j + \left(1 + \frac{14}{9}\left|\frac{a_s}{a} - 1\right|\right)V'(\Delta x_0)t\right\}\right]. \tag{69}$$

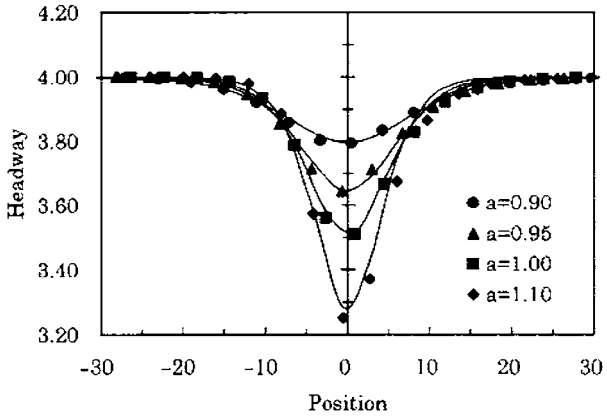

Figure 10. Plot of the headway against position within the soliton density wave. The solid curve indicates the analytical result (69). The circle, triangle, square and diamond points indicate, respectively, the simulation result for $a = 0.90$, 0.95, 1.00 and 1.10.

Figure 10 shows the plot of the headway against position within the soliton density wave. The solid curve indicates the analytical result (69). The circle, triangle, square and diamond points indicate, respectively, the simulation result for $a = 0.90$, 0.95, 1.00 and 1.10. The analytical results are in good agreement with the simulation results near the neutral stability line.

The soliton density appears just above the neutral stability line within the metastable region. According to deviation from the neutral stability line, the soliton density wave becomes unstable. The soliton density wave develops in time to the kink–antikink density wave.

4.3. Modified KdV equation

Kerner and Konhauser (1993) have shown that the single-pulse density wave appears as the traffic jams at high density by simulation of the hydrodynamic model. Bando *et al* (1995) have shown that the traffic jams appear as the kink–antikink density wave in the unstable traffic region by simulation of the optimal velocity model. Later, Komatsu and Sasa (1995) have presented the nonlinear analysis for the optimal velocity model (2). They have derived the modified KdV equation for the traffic jams.

Let us derive the modified KdV equation for the model (1). We note that it is necessary for the optimal velocity function to have a turning point. Otherwise, one cannot derive the modified KdV equation. The perturbation around the critical point $(x_c, 1/\tau_c)$ is considered. For the neighbourhood of the critical point, a small parameter ε is defined as $\varepsilon^2 = 2V'(x_c)\tau - 1$ $(0 < \varepsilon \ll 1)$. By defining the slow variables $X = 2\varepsilon(j + V'(x_c)t)$ and $T = \varepsilon^3 V'(x_c)t/3$, one sets the headway as $\Delta x_j(t) = x_c + \varepsilon(V'(x_c)/|V'''(x_c)|)^{1/2} R(X, T)$. By expanding equation (1) to fifth order of ε, one obtains

$$\varepsilon^4 \left(\frac{\partial R}{\partial T} - \frac{\partial^3 R}{\partial X} + \frac{\partial R^3}{\partial X} \right) + \mathrm{O}(\varepsilon^5) = 0, \tag{70}$$

where $\mathrm{O}(\varepsilon^5)$ is the fifth-order term. Equation (70) is just the modified KdV equation with an $\mathrm{O}(\varepsilon)$ correction term. The modified KdV equation has the kink solution

$$R(X, T) = c^{1/2} \tanh \left[\left(\frac{c}{2} \right)^{1/2} (X - cT) \right]. \tag{71}$$

The correction term $O(\varepsilon^5)$ is necessary to determine the selected value of c. By using the solvability condition, one obtains $c = 6$. In terms of the original parameters, the kink solution is given by

$$\Delta x_j(t) = x_c \pm \left[\frac{6V'(x_c)(2V'(x_c)\tau - 1)}{|V'''(x_c)|}\right]^{1/2} \times \tanh[\{12(2V'(x_c)\tau - 1)\}^{1/2}\{j + V'(x_c)(2 - 2V'(x_c)\tau)t\}]. \quad (72)$$

The kink solution (72) agrees with (57) obtained from the TDGL equation.

The kink solution of the differential equation model (2) is given by

$$\Delta x_j(t) = x_c \pm \left[\frac{5V'(x_c)(2V'(x_c)\tau - 1)}{|V'''(x_c)|}\right]^{1/2} \times \tanh\left[\left\{\frac{5(2V'(x_c)\tau - 1)}{2}t\right\}^{1/2}\left\{j - \frac{5V'(x_c)}{6}(2V'(x_c)\tau - 1)t\right\}\right]. \quad (73)$$

The coefficients of model (1) are different from those of model (2). The theoretical kink solution is in good agreement with the simulation result. Thus, the theoretical result holds for the region of $1 < \tau_c/\tau < 2$ far from the critical point, irrespective of the perturbation of a small deviation from the critical point (Komatsu and Sasa 1995).

We discuss the effect of the next-nearest-neighbour interaction on the traffic jams. We present the theoretical and simulation results of model (7) (Nagatani 1999a, Muramatsu and Nagatani 2000a). The neutral stability condition is given as $\tau = (1 + 2\gamma)/2V'(\Delta x_0)$. By comparing this with (48), the unstable region deceases with increasing γ. The next-nearest-neighbour interaction stabilizes the traffic flow. By applying the above nonlinear analysis to (7), one obtains the kink solution for the traffic jams

$$\Delta x_j(t) = x_c \pm \left[\frac{5V'(x_c)(2V'(x_c)\tau - 1)C_2}{|V'''(x_c)|C_1}\right]^{1/2} \times \tanh\left[\left\{\frac{5(2V'(x_c)\tau - 1)C_3}{2C_1}\right\}^{1/2}\left\{j - \frac{5V'(x_c)C_2}{6C_1}(2V'(x_c)\tau - 1)t\right\}\right], \quad (74)$$

where $C_1 = 1 + 7\gamma + 14\gamma^2$, $C_2 = 1 + 8\gamma + 12\gamma^2$ and $C_3 = 1 + 2\gamma$.

The kink jams become weaker than (73) with increasing strength γ of the next-nearest-neighbour interaction. Thus, the next-nearest-neighbour interaction has the effective effect on the reduction of traffic jams.

5. Comparison with empirical data

Most real traffic data are collected by detectors located at cross sections of the freeway (Kerner and Rehborn 1996a, Nagel *et al* 1998, Kerner 1999a, 2000, 2002, Neubert *et al* 1999, Treiber *et al* 2000). Some data based on aerial photography are obtained to track the trajectories of many interacting vehicles (Treiterer and Taylor 1966, Treiterer and Myers 1974).

Treiterer *et al* have exhibited the spontaneous formation of traffic jams, so-called 'phantom jams', without obvious reason such as a traffic accident or a bottleneck. At an initial stage, vehicles move freely and are well separated from each other. Then, vehicles decelerate, stop for a certain period of time and start again. A typical stop-and-go wave (a traffic jam) is formed. The density wave propagates upstream (oppositely to the moving direction of vehicles).

Kerner and Rehborn (1996a, b, 1997, 1999a, b, 2000) and Kerner (2002) have presented a more detailed analysis of traffic jams on the three-lane highway (A5-North and A5-South

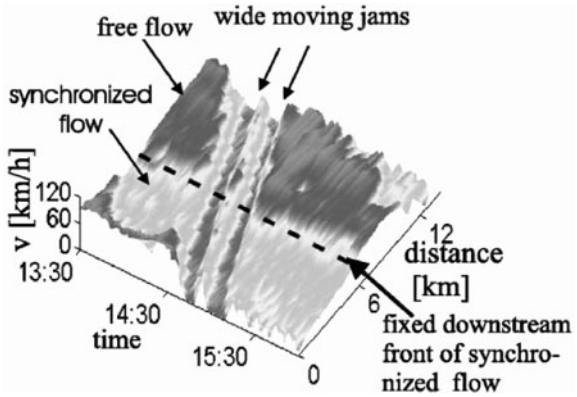

Figure 11. The spatio-temporal evolution of the traffic flow. Wide moving jams and three traffic phases. It is seen that the sequence of two wide jams propagates with a constant velocity through free flow or synchronized flow (Kerner 2002).

in Germany). Figure 11 shows the spatio-temporal evolution of the traffic flow. It is seen that the sequence of two wide jams propagates with a constant velocity through free flow or synchronized flow. Two parallel jams are fully developed and move over a long time periods and road sections. The wide moving jam has an upstream moving localized structure which is restricted by two fronts where the vehicle speed changes sharply. The vehicle speed and the flow rate inside a wide jam are either zero or negligible. There is no influence of the inflow into the jam on the jam's outflow. The wide moving jams possess unique, coherent, predictable and reproducible parameters which do not depend on time and they are the same for different wide moving jams if control parameters (weather and other road conditions) of traffic do not change. These properties are similar to the kink jams or auto-solitons predicted by the nonlinear wave equations. They have found three distinct phases of traffic: free flow (F), synchronized flow (S) and wide moving jam (J). Figure 11 shows the three traffic phases. The diagrams on the top in figure 12 show the plots of average vehicle speed against time for three traffic phases. The diagrams on the bottom in figure 12 show the representations of the related traffic phases on the flow-density plane (Kerner 2002). Possible ways of a theoretical description of the empirical features of the traffic phases synchronized flow and wide moving jam is up to now in a discussion between different scientific groups (Treiber *et al* 2000, Kerner 2002).

Nagel *et al* (1998) have compared the simulation result obtained from the two-lane NaSch model with the empirical data on the two-lane highway measured by Wiedemann (1995). The left column in figure 13 shows the empirical data of flow and lane usage as function of density. The density, flow, velocity and lane usage are measured in units of veh/km/2lanes, veh/h/2lanes, $\mathrm{km\,h^{-1}}$ and %, all averaged over 1 min intervals. The top left plot shows the typical flow-density diagram. At low densities, the flow increases linearly with density until it reaches a maximum $q \approx 3500$ veh/h/2lanes at $\rho \approx 40$ veh/km/2lanes. The addition of vehicles does not change the average velocity and flow is a linear function of density. At high densities, traffic consists irregularly of jam waves and laminar outflow between jams. Data points are arbitrary averaged over these regimes, leading to a larger variability in the measurements. The velocity against density confirms this. There exists an abrupt drop in the average velocity at $\rho \approx 40$ veh/km/2lanes. The lane usage shows a peculiarity. At very low densities, all vehicles are in the right lane as should be expected. With increasing density, more than half of the traffic is on the left lane. At densities above the maximum flow point this reverts to an equal distribution of densities between lanes.

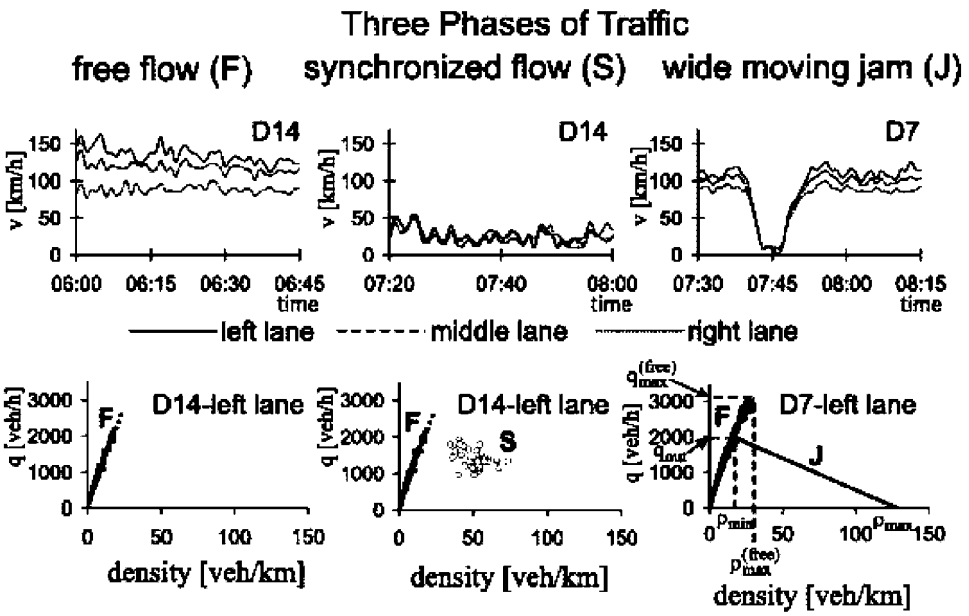

Figure 12. Three distinct phases of traffic: free flow (F), synchronized flow (S) and wide moving jam (J). The diagrams on the top show the plots of average vehicle speed against time for three traffic phases. The diagrams on the bottom show the representations of the related traffic phases on the flow-density plane (Kerner 2002).

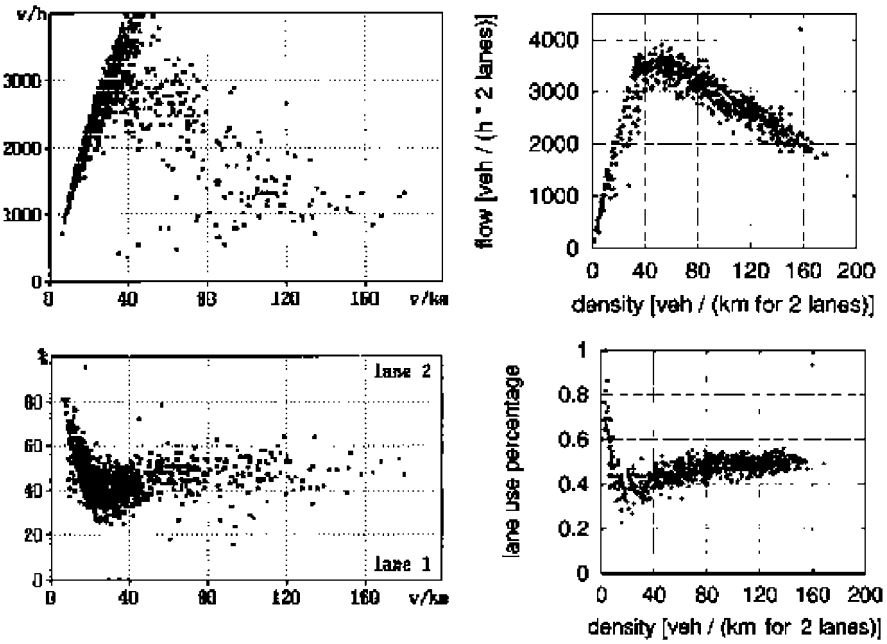

Figure 13. The left column plots show the empirical data of flow (top) and lane usage fraction (bottom) as function of density (Wiedemann 1995). The density, flow, velocity and lane usage fraction are measured in units of veh/km/2lanes, veh/h/2lanes, km h^{-1} and %, all averaged over 1 min intervals. The right column plots show the simulation result obtained by the extended NaSch model to the two lanes (Nagel *et al* 1998).

Nagel *et al* (1998) have extended the NaSch model to the two-lane traffic to take into account the lane changing rule and trucks. They have obtained the simulation result similar to the empirical data. The right column in figure 13 shows the plots of flow (top) and lane usage fraction (bottom) obtained from the simulation against density.

The above results are obtained from time-averaged measurements. It is also useful to analyse statistically the single-vehicle data of highway traffic. By using the single-vehicle data directly, empirical time headway distributions and speed–distance relations can be obtained (Neubert *et al* 1999, Knospe *et al* 2002a). Both quantities yield relevant information about the microscopic states. Figure 14 shows the time-headway distributions of different traffic states at

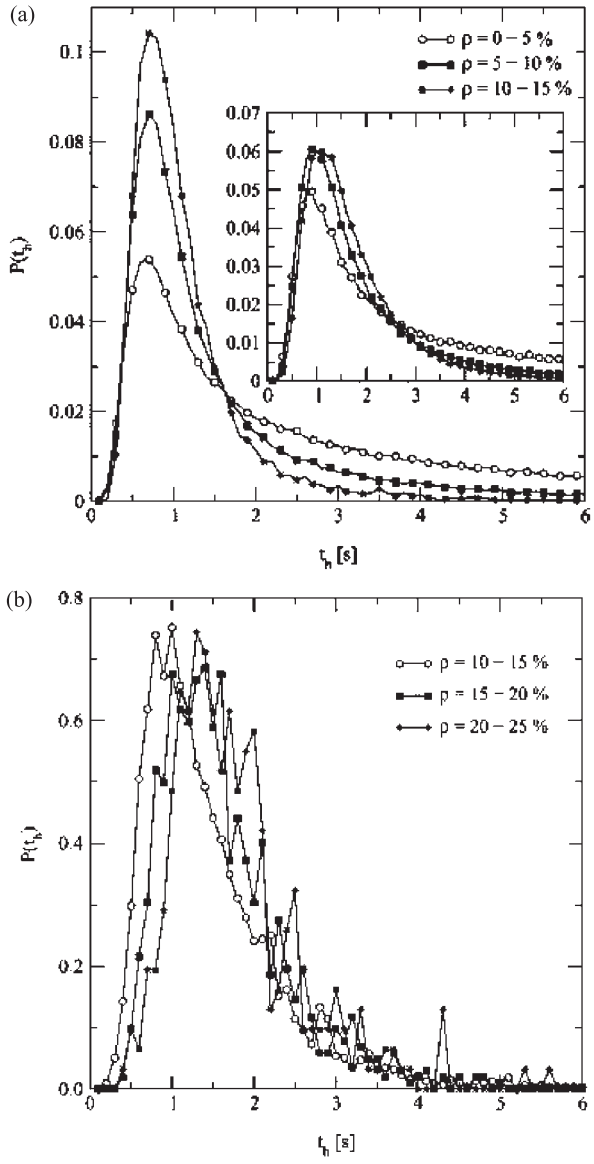

Figure 14. (Continued)

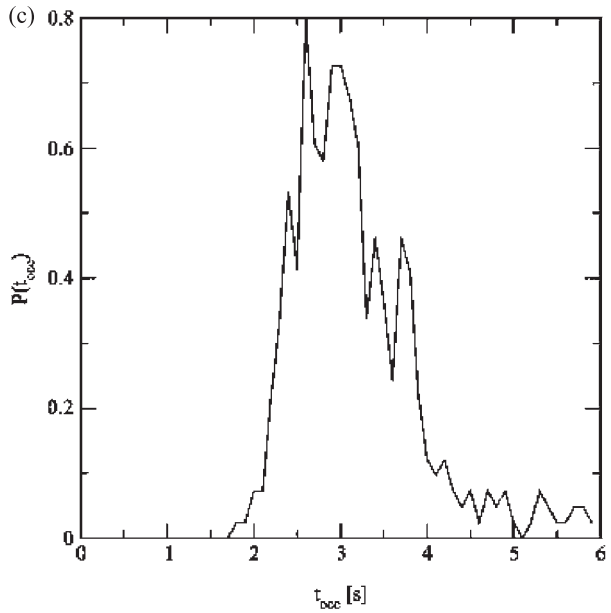

Figure 14. Time-headway distributions of different traffic states at different local densities (Knospe *et al* 2002a). (*a*) Distribution of free flow traffic. (*b*) Distribution of synchronized traffic. (*c*) Distribution of wide moving jams.

different local densities. The distributions of time headway for free traffic, synchronized flow and wide moving jams (congested traffic) are indicated in figure 14 (*a*)–(*c*), respectively. The distribution (*c*) of wide moving jams represents that of the time during which the detector is occupied by a car since the calculation of the accurate time headway is not possible for the car to stop at the detector. The time-headway distributions show a strong dependence on the density.

For the free flow traffic (*a*), the short time behaviour remains nearly unchanged although the width of the distribution decreases. Not only the maximum of the distribution is at about 0.68 s, but also the values of the shortest time headways do not change significantly. In contrast to free flow, the time-headway distribution (*b*) of the synchronized flow shows a non-trivial dependence on the density. While the maximum of the distribution is shifted to larger values ($\approx$1.3 s) and the variance is reduced, small time headways do still exist. The probability of these small time headways decreases with increasing density, whereas the distribution in free flow can simply be rescaled by the density for small times. For wide moving jams, a car at rest needs to accelerate. The distribution (*c*) shows that a car needs a minimum time of about 2 s to accelerate. As a characteristic property of a wide jam, this time determines the escape rate from a jam and thus its outflow.

The most important information for an adjustment of the speed is the accessible distance headway. In the optimal velocity model, this is used as input parameters (Bando *et al* 1995a). A detailed analysis of the speed–distance relationship is important to model traffic flow. Neubert *et al* (1999) have obtained the speed–distance relations from the reduced data set of the single-vehicle data. Figure 15 shows the speed–headway relations for the different traffic states (top and middle) and all states (bottom). The dotted line indicates the optimal velocity function by Bando *et al* (1995b). In the free-flow regime, the function is characterized by a steep increase at small distances corresponding to the short time headways in figure 14 (top). For synchronized states, the asymptotic speed takes a rather small value. When averaging over

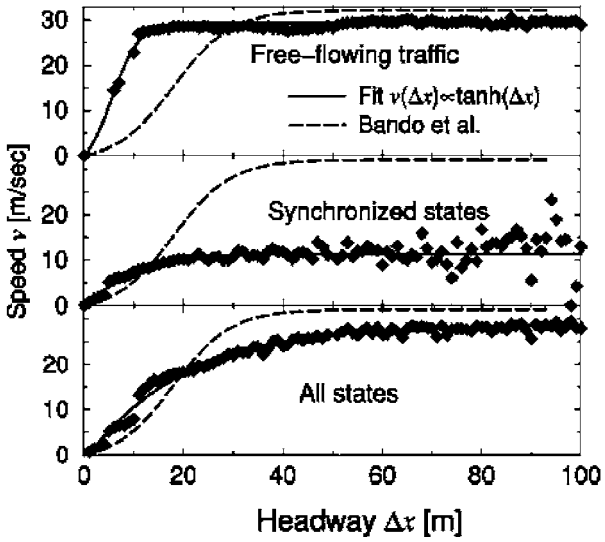

Figure 15. Speed-headway relations for the different traffic states (top and middle) and all states (bottom) (Neubert *et al* 1999). The dotted line indicates the optimal velocity function by Bando *et al* (1995b).

both free-flow and congested states (figure 15, bottom), the asymptotic regime is reached at much larger distances. It is necessary to distinguish between the traffic states in order to get a more precise description of the speed–headway relation.

Figure 16 shows the mean-flow–density relation obtained by using the single-vehicle data. The results for two averaging procedures are displayed. The continuous form (white square points) of the fundamental diagram is obtained by averaging over all flow values of a given density, while the discontinuous shape (black points) is obtained by discriminating between free-flow and synchronized traffic. The continuous stationary fundamental diagram depends on the statistical weight of free-flow and synchronized states. Therefore, it is necessary to distinguish between the different states in order to obtain reasonable results for the stationary fundamental diagram. Here, the constant flow in a wide range of high densities is produced by the bottleneck effect.

Recently, traffic breakdowns behind bottlenecks have attracted considerable attention (Hall and Agyemang-Duah 1991, Daganzo 1996, Kerner and Rehborn 1996b, 1997, Nagatani 1997c, 2000b, Helbing and Treiber 1998a, b, Lee *et al* 1998, 1999, Helbing *et al* 1999, Kerner 2002). Measurements of traffic breakdowns on various freeways suggest that many dynamic aspects are universal and therefore accessible to a physical description (Treiber *et al* 2000). One common property is the capacity drop (typically of the order of 20%) associated with a breakdown, which induces the hysteresis effects and is the basis of applications like dynamic traffic control to avoid the breakdown. In most cases, traffic breaks down upstream of a bottleneck and the congestion has a stationary downstream front at the bottleneck. The types of bottleneck (on-ramps, lane closings, tunnel or uphill gradients) are not necessarily important. Some types of congested traffic have been found and there are extended states with a relatively high flow among them. These states, referred to as synchronized traffic, can be more or less homogeneously flowing or exhibit distinct oscillations in the time series of detector data (Kerner and Rehborn 1996b, 1997, Kerner 2002). The congested traffic flow is very often homogeneous near the bottleneck except for fluctuations but oscillations occur further upstream (Kerner 1998). Also, there is an observation of traffic breakdown to a PLC near on-ramp.

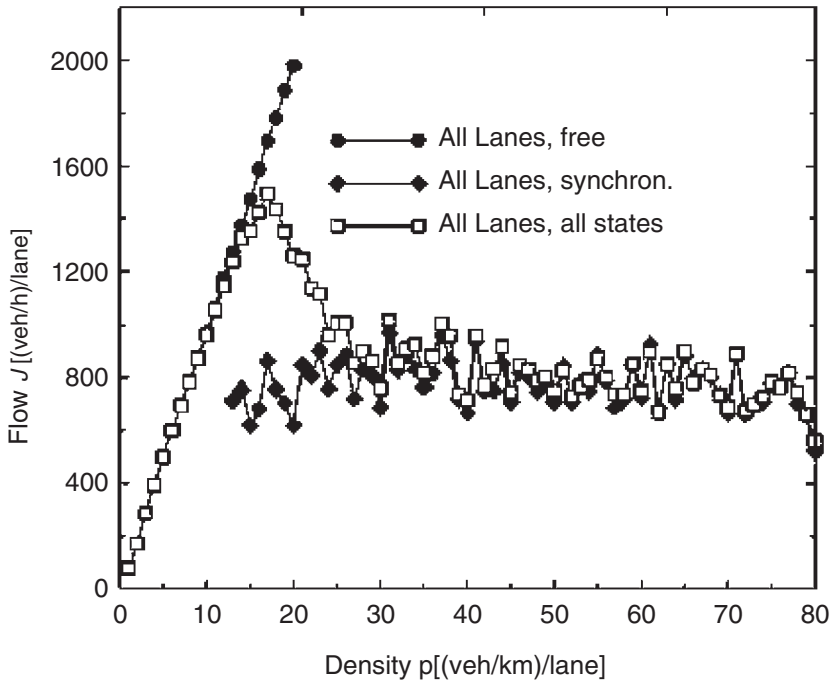

Figure 16. Mean-flow–density relation obtained by the single-vehicle data (Neubert *et al* 1999). The continuous form (white square points) of the fundamental diagram is obtained by averaging over all flow values of a given density, while the discontinuous shape (black points) is obtained by discriminating between free-flow and synchronized traffic.

Treiber *et al* (2000) have presented the detailed empirical data showing different kinds of congested traffic forming near road inhomogeneities. The traffic states are localized or extended, and homogeneous or oscillating. The combined states are observed like the coexistence of MLCs and pinned clusters at road inhomogeneities, or regions of OCT upstream of nearly HTC. The empirical findings are consistent in a recently proposed theoretical phase diagram for traffic near on-ramps (Helbing *et al* 1999). They have simulated the same situations with the use of the IDM where the empirical values are used for the boundary conditions (Treiber *et al* 2000). They have reproduced all empirical observations including the coexistence of states by describing inhomogeneities with local variations of one model parameter.

Figure 17 shows the spatio-temporal plots of the local velocity obtained by Treiber *et al* (2000). The pattern (*a*) shows that the incident induces a breakdown to an extended state of HCT. There exist the small oscillations near the upstream boundary. The downstream front remains fixed at the bottleneck ($x \approx 478$ km), while the upstream front propagates upstream. The vehicles enter the congested region at the upstream front and can accelerate into FT at the downstream front. The pattern (*b*) shows the spatio-temporal plot of the local velocity obtained from the corresponding micro-simulation with upstream boundary conditions of empirical data and homogeneous von Neumann downstream boundary condition. The empirical spatio-temporal pattern (*a*) is in quantitative agreement with the simulated pattern (*b*).

Figure 18 shows the spatio-temporal plots of the smoothed velocity of the oscillating congested state occurring during the rush hour. The pattern (*a*) is obtained from the empirical data where traffic breaks down to oscillating congested state by the bottleneck inhomogeneities of intersections (Treiber *et al* 2000). The pattern (*b*) is obtained from the corresponding

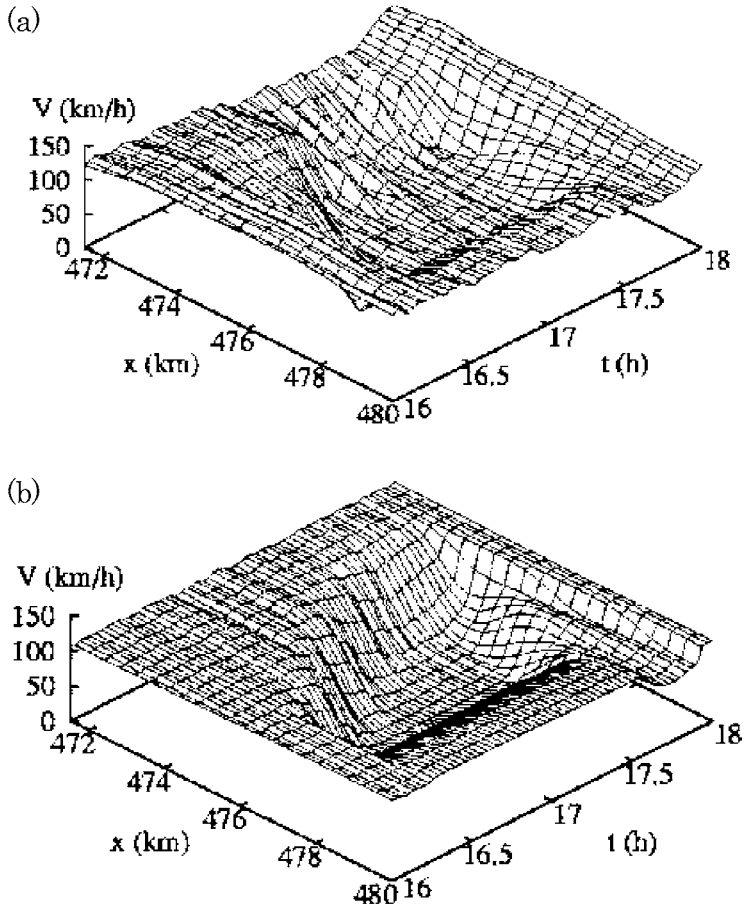

Figure 17. (*a*) Spatio-temporal plot of local velocity obtained from the empirical data of traffic breakdown (Treiber *et al* 2000). This exhibits the extended state of HCT. (*b*) Spatio-temporal pattern obtained from the corresponding microsimulation.

micro-simulation by the use of the empirical boundary conditions. Oscillations with a period of about 12 min are observed. The velocity of OCT state rarely exceeds 50 km h^{-1}, i.e. there is no FT between the clusters. This exhibits the signature of OCT while there is FT between the TSG waves. The downstream front of OCT is fixed at the bottleneck while the upstream front propagates upstream with a constant velocity of 15 km h^{-1}. The simulated spatio-temporal pattern (*b*) shows a quantitative agreement with the empirical pattern (*a*).

Figure 19 shows the spatio-temporal plots of local density for the two MLCs (TSG waves) and PLC observed on the freeway A5 North near Frankfurt (Treiber *et al* 2000). The patterns (*a*) and (*b*) are obtained respectively from the empirical data and the corresponding micro-simulation. The stop-and-go waves are triggered near an intersection. Two stop-and-go waves are separated by FT. Two isolated density waves propagate through FT and do not trigger any secondary waves. This is consistent with MLCs. There also exists a PLC at $x = 479$ km. The simulated pattern (*b*) exhibits the coexistence of pinned and MLCs. This is in quantitative agreement with the observed dynamics.

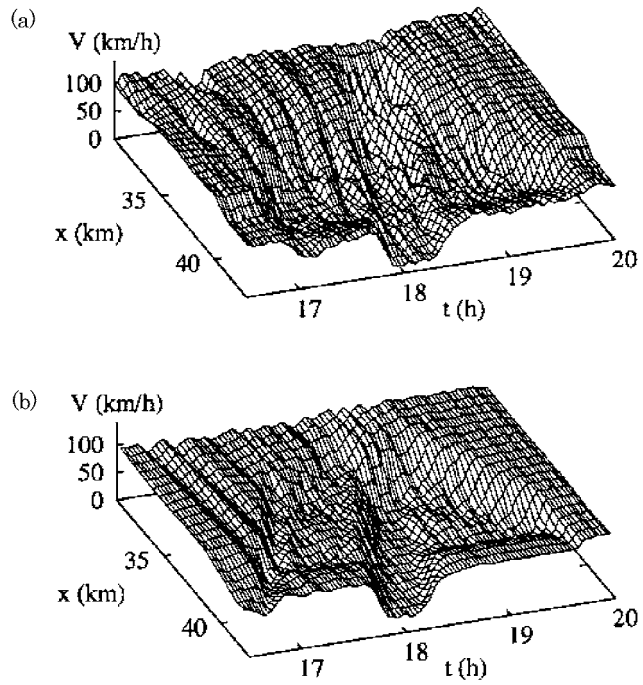

Figure 18. (*a*) Spatio-temporal plot of the smoothed velocity for the oscillating congested state occurring during the rush hour, obtained from the empirical data. Traffic breaks down to oscillating congested state by the bottleneck inhomogeneities of intersections (Treiber *et al* 2000). The pattern (*b*) is obtained from the corresponding microsimulation with the use of the empirical boundary condition.

Kerner (2002) has studied the empirical features of the phase transition from free flow to synchronized flow (the $F \rightarrow S$ transition) at on and off ramps. It has been found that the $F \rightarrow S$ transition is the local first-order phase transition. From the theory and experimental studies of the local first-order phase transition in nonequilibrium system, it is well known that in a lot of cases the induced phase transition occurs rather than the spontaneous phase transition is realized. The induced $F \rightarrow S$ transition can also occur in traffic flows at a bottleneck if the flow rates are high enough for the occurrence of the $F \rightarrow S$ transition in free flow. The $F \rightarrow S$ transition can be induced when a wide moving jam propagates through the bottleneck. The example of the $F \rightarrow S$ transition is shown in figure 20 (Kerner 2002). During the whole time before the moving jam reaches the on ramp, free flow is realized. After the moving jam has passed the on ramp, a synchronized flow is formed at the on ramp. Thus, the $F \rightarrow S$ transition is induced at the on ramp during the jam propagation.

Very recently, Knospe *et al* (2002b) have shown that the desire for smooth and comfortable driving is responsible for the occurrence of synchronized traffic. Using the stochastic CA model, it has been found that the anticipation effects reproduce the empirically observed coexistence of wide moving jams with both free flow and synchronized traffic.

6. Bus-route systems

The bus operation is also a typical many-body system of interacting buses and passengers. The bus-route dynamics is closely related to the traffic flow dynamics in one dimension. If a bus is

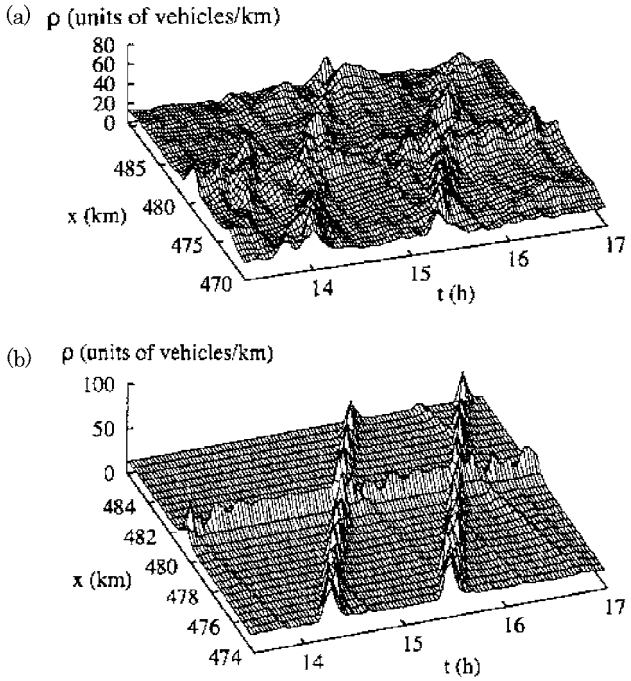

Figure 19. (*a*) Spatio-temporal plot of the density for the two MLCs (TSG waves) and PLC observed on the freeway A5 North near Frankfurt (Treiber *et al* 2000). The pattern (*b*) is obtained from the corresponding microsimulation with the use of the empirical boundary condition.

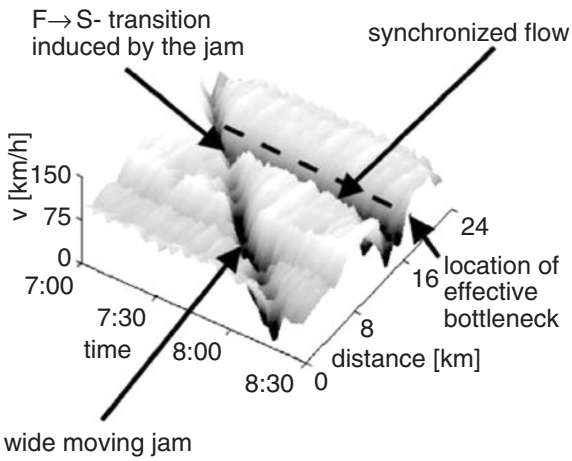

Figure 20. An example of the $F \rightarrow S$ transition (Kerner 2002). During the whole time before the moving jam reaches the on ramp, free flow is realized. After the moving jam has passed the on ramp, a synchronized flow is formed at the on ramp.

delayed by some fluctuation, the time headway (gap) between it and its predecessor becomes larger than the initial time headway because this bus has to pick up more passengers than the initial value. During the period of delay, more passengers will be waiting for the bus. As a result, the bus will get further delayed. The slowly moving delayed bus will slow down the

buses behind it. The bunching transition between an inhomogeneous jammed phase (where the buses bunch together) and a homogeneous phase occurs with varying the initial time headway. Thus, the bus behaviour exhibits the dynamical phase transition similar to the traffic flow.

6.1. Models

The bus-route models have been proposed to investigate the bus behaviour on a bus route. The traffic flow models have been extended to mimic the bus behaviour. Three models have been presented until now: the first is the cellular automaton model (O'loan *et al* 1998, Chowdhury and Desai 2000, Chowdhury *et al* 2000), the second model is the time-headway model of buses (Nagatani 2001a, b) and the third is the car-following model of buses (Nagatani 2000d, Huijberts 2002).

We present the CA model for the bus route (O'loan *et al* 1998). The model is defined on a one-dimensional lattice with periodic boundary conditions. Each lattice site is labelled by a number i running from 1 to L. Each site can be thought of as a bus stop on a bus route. Site i has two binary variables τ_i and ϕ_i associated with it. These variables can be described in the following terms: (i) If site i is occupied by a bus then $\tau_i = 1$; otherwise $\tau_i = 0$. (ii) If site i has passengers on it then $\phi_i = 1$; otherwise $\phi_i = 0$. A site cannot have both $\tau_i = 1$ and $\phi_i = 1$ (i.e. it cannot have a bus and passengers). There are M buses in the system and the bus density $\rho = M/L$ is a conserved quantity. The update rules for the system are as follows: (1) Pick a site i at random. (2) If $\tau_i = 0$ and $\phi_i = 0$ then $\phi_i \to 1$ with probability λ. (3) If $\tau_i = 1$ and $\tau_{i+1} = 0$, define a hopping rate μ as follows: (i) $\mu = \alpha$ if $\phi_{i+1} = 0$; (ii) $\mu = \beta$ if $\phi_{i+1} = 1$, and update $\tau_i \to 0$, $\tau_{i+1} \to 1$ and $\phi_{i+1} \to 0$ with probability μ.

Thus, α is the hopping rate of a bus onto a site with no passengers and β is the hopping rate onto a site with passengers. One takes $\beta < \alpha$, reflecting the fact that buses are slowed down by having to pick up passengers. The probability that a passenger arrives at an empty site is λ. When a bus hops onto a site with passengers, it removes the passengers. The presence of more than one passenger at a site is not forbidden. The extra passengers have no further effect on the dynamics. Once a larger gap opens up between two successive buses, the gap is likely to grow further and the steady state in a finite system consists of a single jam of buses. This is very similar to the Bose–Einstein-condensation-like phenomenon observed earlier in particle-hopping models with quenched random hopping rates (Nagatani 1995, Evans 1996, 1997, Krug and Ferrari 1996, Ktitarev *et al* 1997). The CA model with parallel dynamics has been studied where its connection with NaSch model has been elucidated (Chowdhury and Desai 2000).

We describe the time-headway model in detail. The model is defined on a one-dimensional lattice. Each lattice site is labelled with a number m running from 1 to M. A site represents a bus stop. Buses move on the one-dimensional lattice. Each bus is labelled with a number j running from 1 to N. The distance between bus stop $m-1$ and m is set by L_{m-1}. The model is illustrated schematically in figure 21. The mean velocity of bus j between bus stops $m-1$ and m is defined by $v_j(m-1)$. The arrival time $t_j(m)$ of bus j at bus stop m is given by

$$t_j(m) = t_j(m-1) + \frac{L_{m-1}}{v_j(m-1)}. \tag{75}$$

A bus driver operates his bus in such a manner that his velocity increases or decreases according to the time-headway which is large or small. Assuming that the mean velocity of bus j at bus stop m depends only on the time headway of bus j at the bus stop m, the mean velocity $v_j(m)$ is given by the operation velocity function $V(\Delta t_j(m))$ where the time headway is defined by $\Delta t_j(m) = t_j(m) - t_{j+1}(m)$. The operation velocity is similar to the optimal velocity function

of the car-following model for traffic flow (Bando *et al* 1995, Nagatani 1998). The equation of motion for bus j is described in terms of time headway

$$\Delta t_j(m) = \Delta t_j(m-1) + L_{m-1}\left[\frac{1}{V(\Delta t_j(m-1))} - \frac{1}{V(\Delta t_{j+1}(m-1))}\right], \tag{76}$$

with

$$V(\Delta t_j(m)) = v_{\min} + \tfrac{1}{4}(v_{\max} - v_{\min})[\tanh(\Delta t_j(m) - t_c) + \tanh(t_c)][1 + \exp(-\lambda \Delta t_j(m))], \tag{77}$$

where λ is the rate of arrival of passengers, $v_{\min}$ is the minimal velocity, $v_{\max}$ is the maximal velocity in the limit of $\lambda = 0$ and t_c is the desired time headway. When $\lambda = 0$, the operation velocity is consistent with the optimal velocity function of the traffic model except for $v_{\min} \neq 0$ and the replacement of the distance headway with the time headway. The operation velocity function has the following properties: (1) in the limit of $\lambda = 0$, the velocity increases monotonically with the time headway and (2) the velocity decreases with increasing time headway for small λ and large time headway. The property (1) reflects the fact that when the bus behind catches up with the delayed bus, it should slow down in order to avoid a collision. The property (2) reflects the fact that the bus is delayed more and more with increasing the gap size (time headway) in front of the bus because the delayed bus should pick up more passengers.

Figure 22 shows the plot of equation (77) against time headway for $\lambda = 0.2$, $v_{\min} = 2.0$, $v_{\max} = 4.0$ and $t_c = 2.0$. Thus, the bus-route problem is reduced to its simplest form. In this basic model, each bus stops at all the bus stops. The basic model has been extended to take

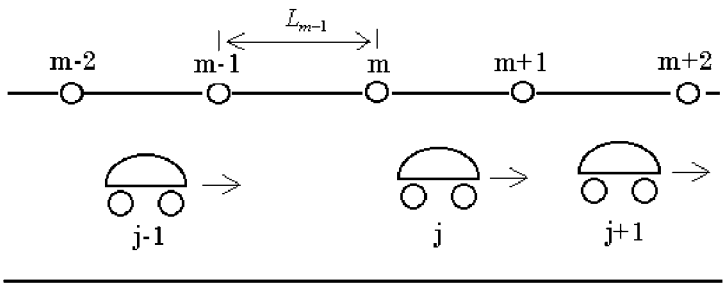

Figure 21. Schematic illustration of the bus-route model.

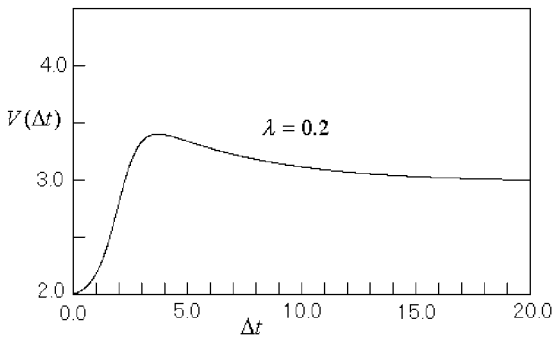

Figure 22. Plot of the operation velocity $V(\Delta t)$ against time headway Δt.

into account no stopping of the delayed bus and the speed up of a non-stopping bus (Nagatani 2001a).

The car-following model of traffic has been extended to the bus-route model directly (Nagatani 2000d). The equation of motion for a bus is the same as the traffic model but the optimal velocity function is different from that of traffic. The car-following model of buses is described by

$$\frac{\mathrm{d}x_j(t+\tau)}{\mathrm{d}t} = V(\Delta x_j(t)), \tag{78}$$

with

$$V(\Delta x_j) = \left(\frac{v_{\max}}{2}\right)\{\beta + (1-\beta)\exp(-\lambda\Delta x_j)\}\{\tanh(\Delta x_j - x_c) + \tanh(x_c)\}, \tag{79}$$

where $x_j(t)$ is the position of bus j at time t, $\Delta x_j(t)$ is the distance headway of bus j at time t, τ is the delay time and λv_a is the rate of arrival of passengers (v_a is the average velocity). This model has the same properties as the time-headway model. The differential equation and difference equation models have also been proposed for the bus-route problem (Nagatani 2000d, Huijberts 2002).

The time-headway model has been extended to take into account the number of on-board passengers within buses (Nagatani 2001b). The extended model is described by the following equation

$$t_j(m) = t_j(m-1) + \frac{L_{m-1}}{v_j(m-1)} + \max[\gamma I_j(m-1), \delta O_j(m-1)], \tag{80}$$

with

$$v_j(m) = V(\Delta t_j(m)) = \frac{v_{\max}}{2}[\tanh(\Delta t_j(m) - t_c) + \tanh(t_c)], \tag{81}$$

where $\max[A, B]$ is the max function: if $A > B$, $\max[A, B] = A$, otherwise $\max[A, B] = B$. The third-term on the right-hand side represents the stopping time at bus stop $m-1$ for passengers to board bus j or get off from bus j. The number of passengers currently boarding bus j at bus stop m is defined by $I_j(m)$. The number of passengers getting off from bus j at bus stop m is defined by $O_j(m)$. It is assumed that the boarding time is proportional to the number of currently boarding passengers and the getting off time is proportional to the number of currently leaving passengers: $\gamma I_j(m)$ and $\delta O_j(m)$.

The number $M_j(m)$ of on-board passengers on bus j at bus stop m is given by

$$M_j(m) = M_j(m-1) + I_j(m-1) - O_j(m-1). \tag{82}$$

It is assumed that the number of currently boarding passengers is proportional to the time headway and the number of currently leaving off passengers is proportional to the total number of on-board passengers

$$I_j(m) = \lambda\Delta t_j(m) \qquad \text{and} \qquad O_j(m) = \mu M_j(m). \tag{83}$$

The extended model treats accurately the bus dynamics since it includes the various terms connecting to the buses and passengers.

6.2. Bunching of buses

The bus-route model (76) exhibits both bunching (kinetic clustering) and jamming transitions. It is assumed that the distance between bus stops is the same for all bus stops: $L_m = \alpha$. Figure 23 shows the plot of the average velocity $v(\Delta t_0)$ as a function of the initial time headway Δt_0 where $\alpha = 12.0$, $t_c = 2.0$, $\lambda = 0.2$, $v_{\min} = 2.0$ and $v_{\max} = 4.0$. The average velocity at bus stop

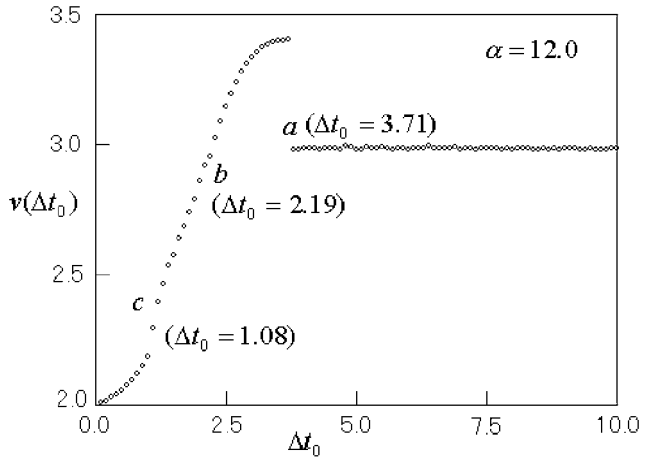

Figure 23. Plot of the average velocity $v(\Delta t_0)$ as a function of the initial time headway Δt_0.

m is defined as $v(\Delta t_0) = (1/N)\sum_{j=1}^{N} V(\Delta t_j(m))$ where $\Delta t_0 = (1/N)\sum_{j=1}^{N} \Delta t_j(m)$. There exist the three discontinuous points labelled by a, b and c. The average velocity increases with the time headway to $\Delta t_0 = 1.08$. At point c, the average velocity increases discontinuously by a small quantity. There is a small gap at point c. Then, the average velocity increases to point b ($\Delta t_0 = 2.19$). At point b, there is a small gap of the velocity. Furthermore, the average velocity increases with time headway to point a. At point a of $\Delta t_0 = 3.71$, the velocity decreases abruptly to $v = 2.98$. In time headway larger than $\Delta t_0 = 3.71$, the velocity remains nearly constant. There are the four distinct dynamic states for the four regions: (a) the bunching phase, (b) the homogeneous free phase, (c) the kink jam phase and (d) the homogeneous congested phase. The free, kink jam and congested phases are the same as those of the traffic flow. The bunching phase is characteristic of the bus-route system. The blocking of the delayed bus induces the kinetic clustering (bunching) of buses behind. This is due to the exponential factor of the operation velocity function. Figure 24 shows the time evolution of time headway for the bunching phase. The fluctuations at an initial stage grow accordingly as buses proceed. The delayed buses catch up with the bus behind. In time, the time headways of some buses increase with time.

We show the phase diagram (region map) of the four distinct dynamical states in figure 25. The phase diagram is represented in the space $(\Delta t_0, 1/\alpha)$. The inhomogeneous bunching phase, the homogeneous free phase, the coexisting phase (kink jam phase) and the homogeneous congested phase are indicated by IB, HF, COE and HCT, respectively.

The phase boundaries are derived with the use of the linear stability analysis. The solid curves indicate the phase boundaries obtained by the linear stability analysis. The circles indicate those obtained by simulation. The linear stability theory is applied to the time-headway model (76) with operation velocity (77). Let $y_j(m)$ be small deviations from the homogeneous bus flow: $\Delta t_j(m) = \Delta t_0 + y_j(m)$. Then, the linear equation is obtained

$$y_j(m) = y_j(m-1) + \frac{\alpha V'(\Delta t_0)}{V(\Delta t_0)^2}\{y_{j+1}(m-1) - y_j(m-1)\}, \tag{84}$$

where $V'(\Delta t_0)$ is the derivative of operation velocity at Δt_0. By expanding $y_j(m) = Y\exp(\mathrm{i}kj + zm)$, one obtains

$$e^z = 1 + \frac{\alpha V'(\Delta t_0)}{V(\Delta t_0)^2}(e^{\mathrm{i}k} - 1). \tag{85}$$

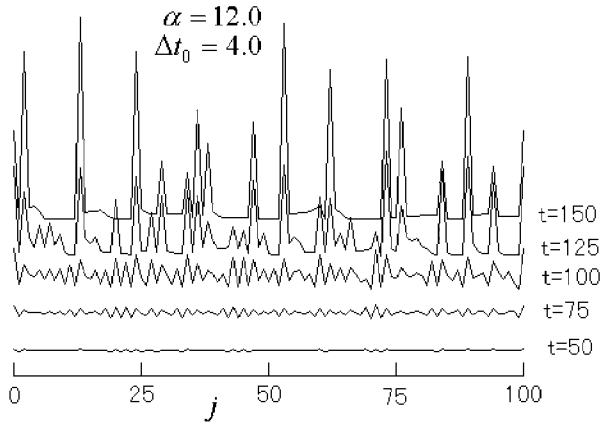

Figure 24. Time evolution of time headway for the bunching phase.

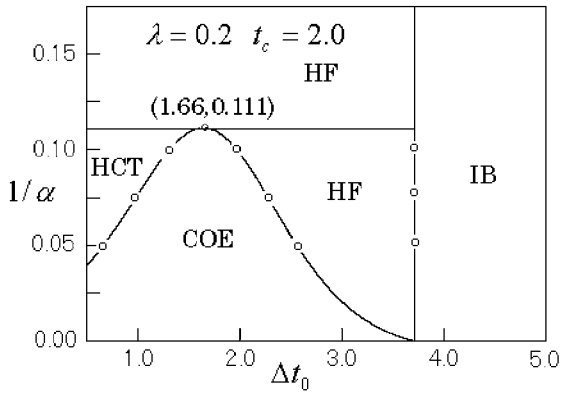

Figure 25. Phase diagram in the space $(\Delta t_0, 1/\alpha)$. (a) The inhomogeneous bunching phase, (b) the homogeneous free phase, (c) the coexisting phase (kink jam phase) and (d) the homogeneous congested phase are indicated by IB, HF, COE and HCT respectively.

By solving equation (85) with z, one finds the unstability condition for small disturbances of long wavelengths:

$$V'(\Delta t_0) < 0, \tag{86}$$

or

$$V'(\Delta t_0) > 0 \qquad \text{and} \qquad \alpha > \frac{V(\Delta t_0)^2}{V'(\Delta t_0)}. \tag{87}$$

The unstable condition (87) is similar to that of the car-following model of traffic with the replacement of the inverse of bus-stop distance α by the sensitivity a. The neutral stability line $\alpha = V(\Delta t_0)^2/V'(\Delta t_0)$ for $V'(\Delta t_0) > 0$ presents the jamming transition curve among HF, COE and HCT phases. The unstability condition (86) is characteristic of the bus-route system. The unstability (86) occurs due to the delay of a bus induced by a large gap. The neutral stability condition $V'(\Delta t_0) = 0$ gives the transition line between IB and HF phases.

6.3. Delay of a recurrent bus

In a recurrent bus problem on a circular route with many bus stops, a bus interacts with passengers waiting on bus stops (Nagatani 2001c). With increasing passengers waiting on bus

stops, a bus slows down due to the long time taken for boarding by the awaiting passengers. The interaction between buses does not exist in the single recurrent bus problem but the dynamical phase transition between the delay and schedule-time phases occurs by interaction with passengers on bus stops.

We present the basic model of a recurrent bus on a circular route. There are M bus stops on the circular route. A recurrent bus starts at bus stop $m = 1$, moves around the route and stops at all the bus stops. A bus stop is represented by a lattice site labelled by number m running from 1 to M. The arrival time $t(m, n+1)$ on bus stop m at number $n+1$ of rotation is given by the summation of the stopping time (for new passengers to board the bus) and the moving time between a bus stop and its next bus stop over all the bus stops. The equation of motion is described by

$$t(m,n+1) = t(m,n) + \sum_{l=1}^{m-1} F(\Delta t(l,n+1)) + \sum_{l=1}^{m-1} \frac{L_l}{V(\Delta t(l,n+1))} + \sum_{l=m}^{M} F(\Delta t(l,n)) + \sum_{l=m}^{M} \frac{L_l}{V(\Delta t(l,n))}, \tag{88}$$

where the function F is the stopping time at a bus stop for new passengers to board the bus and the function V is the average speed of the bus between a bus stop and its next bus stop.

The currently boarding passengers on a bus stop increase with the recurrence time. The boarding time is proportional to the power of recurrence time:

$$F(\Delta t(m,n)) = \gamma \Delta t(m,n)^{\alpha}, \tag{89}$$

where recurrence time is defined by $\Delta t(m,n) = t(m,n) - t(m,n-1)$.

Dividing time by the characteristic time $L/v_{\min}$, the M simultaneous equations of the dimensionless recurrence time are obtained

$$\Delta T(m,n+1) = \sum_{l=1}^{m-1} \Gamma \Delta T(l,n+1)^{\alpha} + \sum_{l=1}^{m-1} \frac{L_l/L}{V_e(\Delta T(l,n+1))} + \sum_{l=m}^{M} \Gamma \Delta T(l,n)^{\alpha} + \sum_{l=m}^{M} \frac{L_l/L}{V_e(\Delta T(l,n))}, \tag{90}$$

where $L = \sum_{l=1}^{M} L_l$ is the length of the circular route, $\Delta T = v_{\min}\Delta t/L$, $V_e = V/v_{\min}$ and $\Gamma = \gamma(v_{\min}/L)^{1-\alpha}$.

Figure 26 shows the plot of the recurrence time at bus stop $m = 1$ against rotation number n for various initial values where $\alpha = 2.0$, $\Gamma = 0.02$ and $V_e(\Delta T) = 1$. The diagram (a)

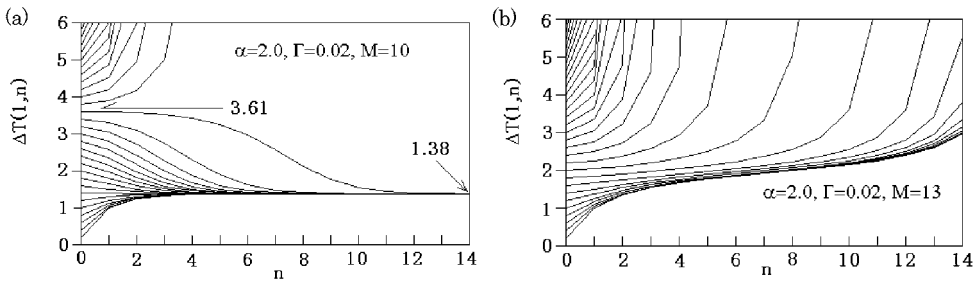

Figure 26. Plot of recurrence time $\Delta T(1,n)$ at bus stop $m = 1$ against rotation number n for various initial value $\Delta T(1,0)$. (a) $M = 10$. (b) $M = 13$.

indicates the flow in the parameter space $(n, \Delta T(1, n))$ for bus stop number $M = 10$. When the initial value $\Delta T(1, 0)$ is less than 3.61, the recurrence time approaches to the fixed point 1.38 with increasing n. The bus can move on schedule time 1.38. If $\Delta T(1, 0)$ is higher than 3.61, the recurrence time diverges with n. The bus slows down more and more with rotation number n. The dynamical phase transition between the delay and schedule-time phases occurs at $\Delta T(1, 0) = 3.61$ for $M = 10$. The diagram (*b*) indicates the flow in the parameter space for bus-stop number $M = 13$. Even if the recurrence time starts from any initial value $\Delta T(1, 0)$, the recurrence time diverges with increasing n. Thus, if the number M of bus stops is larger than the critical value, the bus always delays and cannot move on the schedule time.

Figure 27 shows the phase diagram (region map) in the space $(M, \Delta T(1, 0))$. The circle indicates the transition point between the delay and schedule-time phases. The delayed phase appears at the hatched region. The transition line decreases with increasing M. If the bus-stop number is larger than the critical value $M = 13$, the bus always delays with time and never moves on the schedule time.

We present a simple nonlinear map to approximate equation (90). The recurrence time $\Delta T(m, n)$ at bus stop m is replaced with an effective (or mean) recurrence time $\Delta T(n)$. The M simultaneous equations reduce to a nonlinear equation of a single variable:

$$\Delta T(n+1) = M\Gamma \Delta T(n)^{\alpha} + \frac{1}{V_e(\Delta T(n))}. \tag{91}$$

This is a typical one of the nonlinear map. For $\alpha = 2.0$ and $V_e = 1.0$, the map has the two fixed points if the following condition is satisfied: $4M\Gamma < 1.0$.

Then, the fixed points are given by $\Delta T_{1,f} = (1.0 - \sqrt{1.0 - 4M\Gamma})/2M\Gamma$ and $\Delta T_{2,f} = (1.0 + \sqrt{1.0 - 4M\Gamma})/2M\Gamma$. The fixed point $\Delta T_{1,f}$ is stable and the fixed point $\Delta T_{2,f}$ is unstable. When then $4M\Gamma = 1.0$, there is a single fixed point. For $4M\Gamma > 1.0$, there are no fixed points. Figure 28 shows the plot of map (91). The plots (*a*) and (*b*) indicate the maps for $M = 10$ and $M = 15$, respectively. The map of $M = 10$ has the two fixed points: 1.382 and 3.618. The basin of attraction is given by $\Delta T(0) < 3.618$. The phase boundary of the schedule-time phase is given by the attraction basin. The basin of map (91) is indicated by the solid line in figure 27. Figure 29 shows the plot of transition line (basin of attraction) against

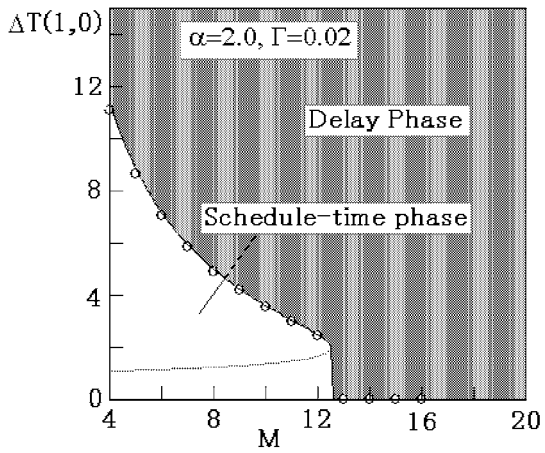

Figure 27. Region map in the space $(M, \Delta T(1, 0))$. The hatched region indicates the delay phase and the other region the schedule-time phase. The solid line represents the transition line obtained from the simple nonlinear map. The dotted line indicates the schedule time.

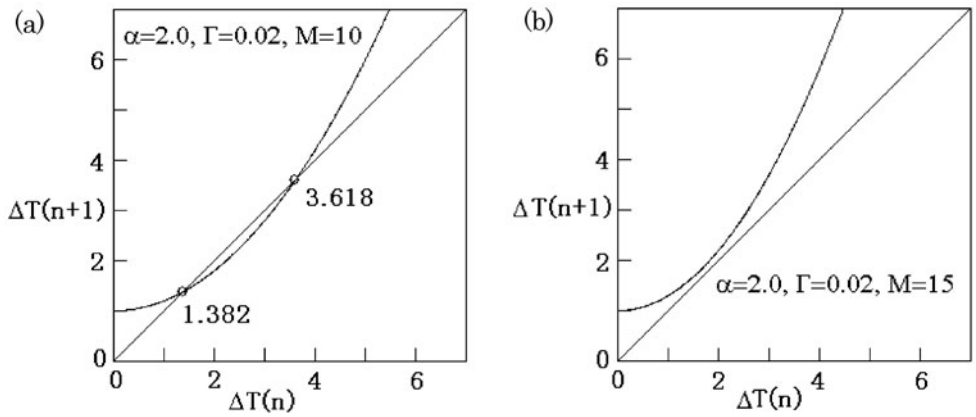

Figure 28. Plot of map (91). The plots (*a*) and (*b*) indicate the maps for $M = 10$ and $M = 15$, respectively.

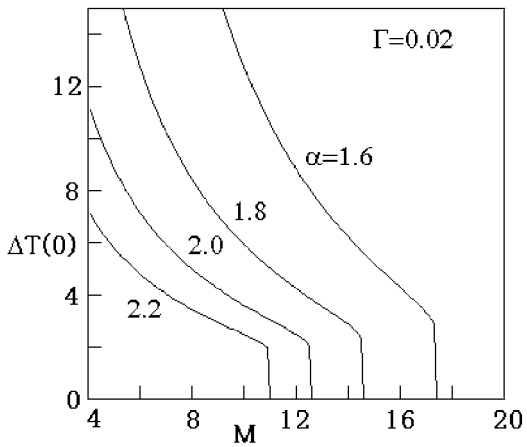

Figure 29. Plot of transition line (basin of attraction) against M for $\alpha = 1.6, 1.8, 2.0, 2.2$ where $\Gamma = 0.02$.

M for $\alpha = 1.6, 1.8, 2.0, 2.2$ where $\Gamma = 0.02$. With decreasing exponent α, the region of the schedule-time phase is enlarged for the basin to expand. Thus, the dynamical behaviour of a recurrent bus can be described in terms of the nonlinear map.

7. Pedestrian flow

This section presents the models and characteristic properties needed for understanding the pedestrian flow. To know the properties of pedestrian flow is important in our life. Especially, it will be necessary to know the flow rate of pedestrian. Pedestrian flow is a kind of many-body system of strongly interacting persons. The pedestrian flow dynamics is closely connected with the traffic flow. The traffic flow is one dimensional but the pedestrian flow is two dimensional. The granular flow is also connected to the pedestrian flow.

Henderson (1971, 1974) has conjectured that pedestrian crowd behaves similarly to gases or fluids. In the gas kinetic or hydrodynamic approaches, it will be necessary to contain the particular interactions between persons. The pedestrian theoretical approaches are developing currently. For practical applications, a direct simulation of individual persons is needed. The recent researches are based on the microscopic simulation models of crowd flow.

When the crowd concentrates to the exit or entrance, the clogging occurs at the exit or entrance, the flow rate saturates and the jammed states of people appear. The jammed states are similar to those observed in traffic flow. The jamming transition between the free flow and jammed state also occurs with increasing persons (Fukui and Ishibashi 1999, Muramatsu *et al* 1999, Helbing *et al* 2000a, b, Klupfel *et al* 2000, Sugiyama *et al* 2001, Schadschneider 2001, Schreckenberg and Sharma 2001).

7.1. Models

In the simulation model, it is important to take into account both excluded-volume effect and preferential direction of walkers. A few models have been presented for simulating the pedestrian flow. One is the lattice-gas model of biased-random walkers which is also a kind of the stochastic CA (Muramatsu *et al* 1999, Muramatsu and Nagatani 2000b, c). The other is the behavioural force model, which is a kind of molecular dynamic simulation models (Helbing 1991, 1996c, 1997a, 1998, 2001, Helbing and Molnar 1995, 1997, Helbing *et al* 2000a, b). Here, we present the characteristic behaviour of pedestrian crowd obtained by using the biased-random walkers. A pedestrian is mimiced by a biased-random walker. The pedestrian model is a modified version of the lattice gas model used in the DLA simulation (Stanley and strowsky 1986, Vicsek 1992, Barabasi and Stanley 1995, Meakin 1998). The pedestrian flow model is defined on the square lattice. Each walker moves to the preferential direction with no back step. The preferential direction of walkers is toward the exit. Each site contains only a single walker. The walker is inhibited from overlapping on the site. The walker does not move to the nearest neighbour occupied by other walkers. Thus the excluded-volume effect is taken into account. A bias (drift) is applied to the preferential direction for random walkers. A walker moves according to and depending on the configurations. Figure 30 shows all possible configurations of a walker where a walker prefers to move right. An arrow points possibly hopping direction. The cross point indicates the site occupied by the other walker. The transition probabilities of the walker depend on each configuration.

The unidirectional pedestrian flow is described by the mean-field rate equation (Nagatani 2001d). We set the preferential direction as x-axis. We apply the conservation law of probability $P(i, j; t)$ of a walker existing on a site (i, j) at time t to the process. We denote the transition probabilities from site (i, j) to the nearest neighbours as $p_{t,x}(i, j; t)$, $p_{t,y}(i, j; t)$ and $p_{t,-y}(i, j; t)$. The probability $P(i, j; t+1)$ of a walker existing on site (i, j) at time $t+1$ is described by the following:

$$\begin{aligned} P(i, j; t+1) = {} & p_{t,x}(i-1, j; t)P(i-1, j; t) + p_{t,-y}(i, j+1; t)P(i, j+1; t) \\ & + p_{t,y}(i, j-1; t)P(i, j-1; t) - \{p_{t,y}(i, j; t) + p_{t,-y}(i, j; t) \\ & + p_{t,x}(i, j; t)\}P(i, j; t). \end{aligned} \tag{92}$$

The first-term on the right-hand side represents the probability flowing into site (i, j) from site $(i-1, j)$. The second (third)-term indicates the probability flowing into site (i, j) from site $(i, j+1)$ (site $(i, j-1)$). The fourth-term represents the probability flowing out from site (i, j) to the nearest neighbours $(i+1, j)$, $(i, j+1)$ and $(i, j-1)$. At a mean-field approximation,

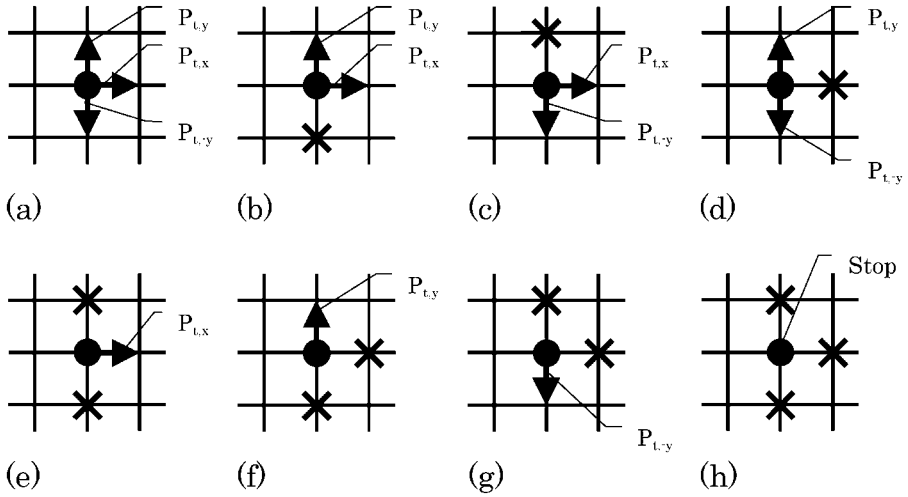

Figure 30. All possible configurations of a walker on the square lattice. The full circle indicates a walker. The cross point indicates the site occupied by the other walker.

the transition probabilities are given by

$$\begin{aligned}
p_{t,x}(i-1,j;t) &= \{1-P(i,j;t)\}\left\{D+\frac{1-D}{3}\right\},\\
p_{t,-y}(i,j+1;t) &= \{1-P(i,j;t)\}\frac{1-D}{3},\\
p_{t,y}(i,j-1;t) &= \{1-P(i,j;t)\}\frac{1-D}{3},\\
p_{t,x}(i,j;t) &= \{1-P(i+1,j;t)\}\left\{D+\frac{1-D}{3}\right\},\\
p_{t,y}(i,j;t) &= \{1-P(i,j+1;t)\}\frac{1-D}{3},\\
p_{t,-y}(i,j;t) &= \{1-P(i,j-1;t)\}\frac{1-D}{3}.
\end{aligned} \tag{93}$$

Here, D is the strength of drift for a based-random walker (Muramatsu *et al* 1999). We assume that the transition probability is proportional to the probability $1-P$ with which a walker does not exist on a nearest neighbour. The excluded-volume effect is taken into account by the probability $1-P$.

We describe the behavioural (or generalized) force model proposed by Helbing *et al* (2000a) to model the collective phenomenon of escape panic in the framework of self-driven many-particle systems. The model of the crowd dynamics of pedestrians is particularly suited to describing the fatal build up of pressure observed during panics. They assume a mixture of socio-psychological and physical forces influencing the behaviour in a crowd: each of N pedestrians i of mass m_i likes to move with a certain desired speed v_i^0 in a certain direction $\boldsymbol{e}_i^0$ and therefore, tends to correspondingly adapt his or her actual velocity $\boldsymbol{v}_i$ with a certain characteristic time τ_i. Simultaneously, he or she tries to keep a velocity-dependent distance from other pedestrians j and walls W. This is modelled by interaction forces $\boldsymbol{f}_{ij}$ and $\boldsymbol{f}_{iW}$, respectively. The change of velocity in time t is then given by the acceleration equation

$$m_i\frac{\mathrm{d}\boldsymbol{v}_i}{\mathrm{d}t} = m_i\frac{v_i^0(t)\boldsymbol{e}_i^0(t)-\boldsymbol{v}_i(t)}{\tau_i} + \sum_{j(\neq i)}\boldsymbol{f}_{ij} + \sum_W \boldsymbol{f}_{iW}, \tag{94}$$

while the change of position $\boldsymbol{r}_i(t)$ is given by the velocity $\boldsymbol{v}_i(t) = \mathrm{d}\boldsymbol{r}_i/\mathrm{d}t$. The psychological tendency of two pedestrians i and j to stay away from each other is described by a repulsive interaction force $A_i \exp[(r_{ij} - d_{ij})/B_i]\boldsymbol{n}_{ij}$, where A_i and B_i are constants. $d_{ij} = \|\boldsymbol{r}_i - \boldsymbol{r}_j\|$ denotes the distance between the pedestrians' centres of mass and $\boldsymbol{n}_{ij} = (\boldsymbol{r}_i - \boldsymbol{r}_j)/d_{ij}$ is the normalized vector pointing from pedestrian j to i. The pedestrians touch each other if their distance d_{ij} is smaller than the sum $r_{ij} = (r_i + r_j)$ of their radii r_i and r_j. In this case, two additional forces are introduced for understanding the particular effects in panicking crowd: a body force $\boldsymbol{f}_{b,ij}$ and a sliding friction force $\boldsymbol{f}_{s,ij}$. In summary, one has

$$\boldsymbol{f}_{ij} = A_i \exp\left[\frac{r_{ij} - d_{ij}}{B_i}\right]\boldsymbol{n}_{ij} + \boldsymbol{f}_{b,ij} + \boldsymbol{f}_{s,ij}, \tag{95}$$

where $\boldsymbol{f}_{b,ij}$ and $\boldsymbol{f}_{s,ij}$ are zero if the pedestrians do not touch each other.

The interaction with the walls is treated analogously. The interaction force with the wall is given by

$$\boldsymbol{f}_{iW} = A_i \exp\left[\frac{r_i - d_{iW}}{B_i}\right]\boldsymbol{n}_{iW} + \boldsymbol{f}_{b,iW} + \boldsymbol{f}_{s,iW}. \tag{96}$$

The generalized force model describes accurately the pedestrian dynamics but large computational time is taken.

7.2. From free flow to clogging

We describe the model of pedestrian flow in a channel with a bottleneck under open boundary condition (Tajima *et al* 2001). The channel is represented by the square of $L \times W$ sites where L is the length of the channel and W is the width of the channel. A bottleneck is positioned on the centre of the channel. The hole of the bottleneck has the width d. Walkers go into the channel from the left boundary (entrance), go through the bottleneck and go out to the right boundary (exit). The density of walkers on the left boundary is set by a constant value p_1. When the walker arrives at the right boundary, it is removed from the channel. If the walker arrives at the wall, it is reflected by the wall and never let out through the wall.

Figure 31 shows the schematic illustration of the pedestrian flow in a channel with a bottleneck. A full circle represents a walker. Initially, walkers are randomly distributed at the entrance boundary on the left-hand side. The walkers move through the bottleneck towards the exit, according to the above transition rule. On the unit time step, all walkers in the channel

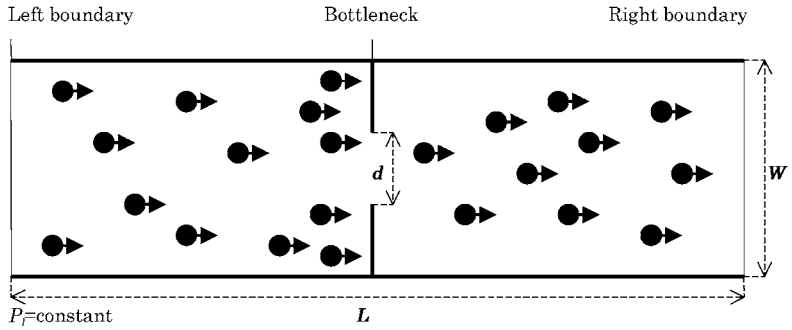

Figure 31. Schematic illustration of the pedestrian channel flow going through a bottleneck. A circle represents a walker. Each walker moves towards the exit on the right-hand side without back step. The length and width of the channel are L and W. The bottleneck width is d.

are updated only once: the update procedure is the random sequential rule. In this model, the pedestrian flow in the channel is reduced to its simplest form.

The pedestrian flow rate exhibits a characteristic property. Figure 32(*a*) shows the plots of mean flow rate (current) J against entrance density p_l for various values of bottleneck width d where the channel length is $L = 200$, the channel width is $W = 40$ and the drift is $D = 0.7$. Figure 32(*b*) indicates the plot of the mean velocity $\langle v \rangle$ against the entrance density p_l. The

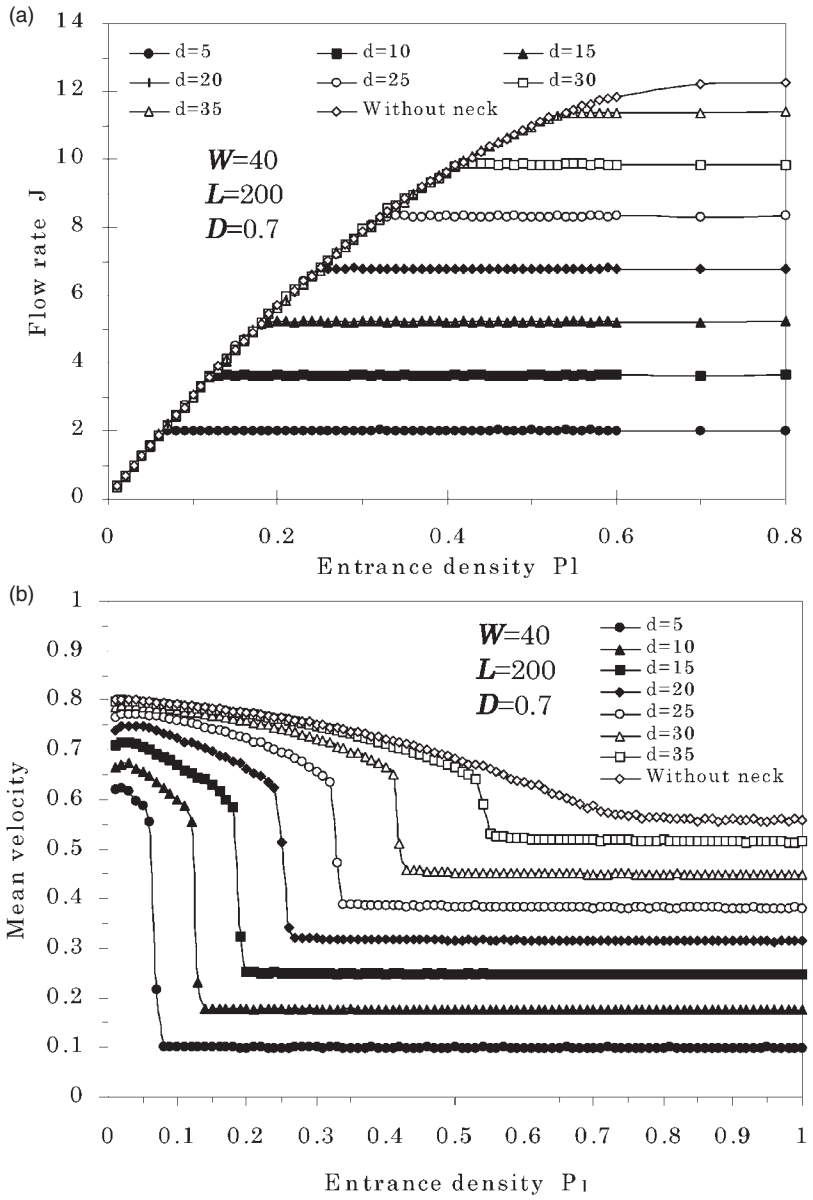

Figure 32. (*a*) Plots of mean flow rate J against entrance density p_l for $d = 5$, 10, 15, 20, 25, 30, 35 where the channel length is $L = 200$, the channel width is $W = 40$, and the drift is $D = 0.7$. (*b*) Plots of mean velocity $\langle v \rangle$ against entrance density p_l.

mean velocity $\langle v \rangle$ of walkers moving in a unit time interval is defined to be the value of the number of moving walkers divided by the total number of walkers existing in the channel. The flow rate increases with entrance density $p_{\rm l}$ and saturates at a critical density $p_{\rm c}$. The flow rate keeps a constant value at larger density than the critical density. This saturation is due to the clogging of walkers at the bottleneck. When the clogging occurs, walkers go through the bottleneck with a constant value of mean flow rate. At the critical density, the mean velocity of walkers decreases abruptly to the low value. One finds that a dynamical phase transition occurs from the free flow to the clogging flow. The critical density increases with the bottleneck width d. The saturated flow rate also increases with the bottleneck width d.

The saturated flow rate $J_{\rm s}$ scales as follows:

$$J_{\rm s} \propto d^{0.93\pm0.02}, \tag{97}$$

where d is the bottleneck width. The scaling of the saturated flow rate has been found in the granular flow (Jaeger and Nagel 1996, Clement *et al* 2000). The scaling exponent 0.93 is less than 1.5 (2.5) in the two(three)-dimensional granular flow. The critical density is given by the point changing from the free flow to the clogging flow. The critical density $p_{\rm c}$ scales as

$$p_{\rm c} \propto \left(\frac{d}{W}\right)^{1.16\pm0.01}. \tag{98}$$

This scaling has not been found in the granular flow. Based on the above scaling forms (97) and (98), one plots the scaled flow rate $J/d^{0.93}$ against the scaled density $p_{\rm l}/(d/W)^{1.16}$ in figure 33 using the data in figure 32(*a*). One finds that data collapses on a single curve for any density. Thus, the pedestrian flow at a bottleneck exhibits the scaling behaviour.

The pedestrian flow with a bottleneck has been analysed by the mean-field rate equation (92) (Nagatani 2001d). The two-dimensional pedestrian flow is approximated

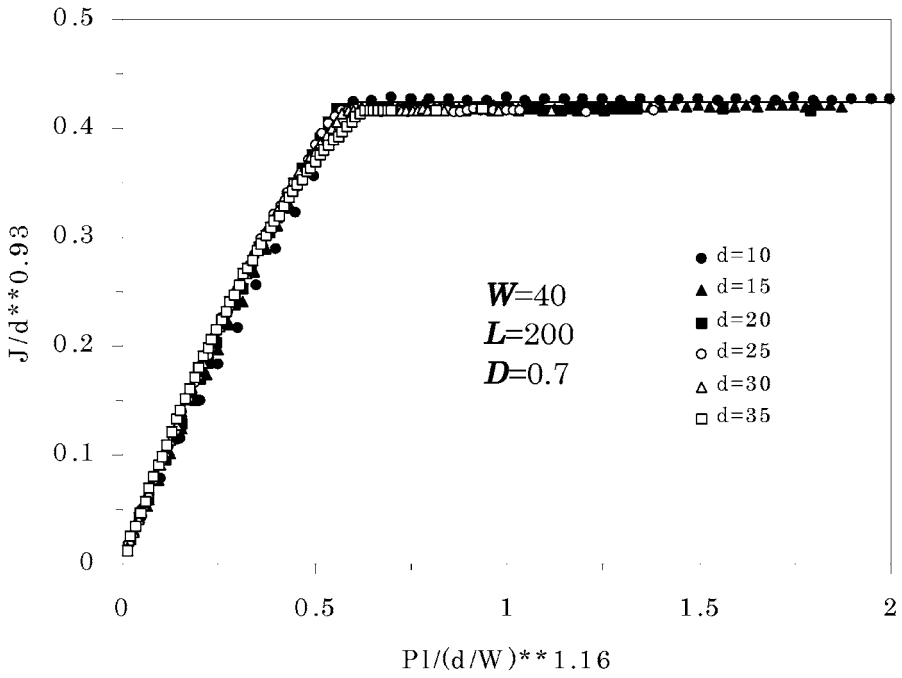

Figure 33. Plot of the scaled flow rate $J/d^{0.93}$ against the scaled density $p_{\rm l}/(d/W)^{1.16}$ for data in figure 32(*a*).

successfully by the one-dimensional mean-field theory. The dynamical transition from the free flow to the clogging flow exhibits the dynamical behaviours similar to those of the asymmetric simple exclusion process with a blockage (Janowsky and Lebowitz 1992, 1994, Popkov and Schutz 1999, Schutz 2000). The free and clogging flows of pedestrian correspond to the low-density and high-density phases of the asymmetric simple exclusion process, respectively.

7.3. Escape flow of crowd

We describe the model of the crowd flow going outside a hall (Tajima and Nagatani 2001). Helbing *et al* (2000a) have studied the escape panic by using the generalized force model (94). The computer simulation of escape panic is a pioneer's work from the point of view of physics. Here, we mimic the crowd flow by the use of the pedestrian lattice gas model. The crowd flow model is defined on the square lattice. The hall is represented by the square of $L \times L$ sites where L is the length of the hall. The hall has a single exit with width W. We assume that people (walkers) are randomly distributed, initially ($t = 0$), over the square space of hall. At the next time ($t > 0$), all walkers move toward the exit. In time, walkers go outside the hall.

Figure 34 shows the schematic illustration of the crowd flow going, through the exit, outside the hall. A circle represents a walker. Each walker moves to the preferential direction with no back step. The preferential direction of walkers is towards the exit. An arrow indicates the preferential direction. All arrows direct to the centre of the exit except for the walkers within the square *abcd*. The arrows of walkers existing within the square *abcd* direct normally to the exit. Each site contains only a single walker. A bias (drift) is applied to the preferential direction for random walkers. The strength of drift for a walker depends on the position of walker since the preferential direction to the exit varies with the position of walker. Accordingly as a walker moves toward the exit, the drift direction changes from position to position. In this model, the crowd flow going outside the hall is reduced to its simplest form.

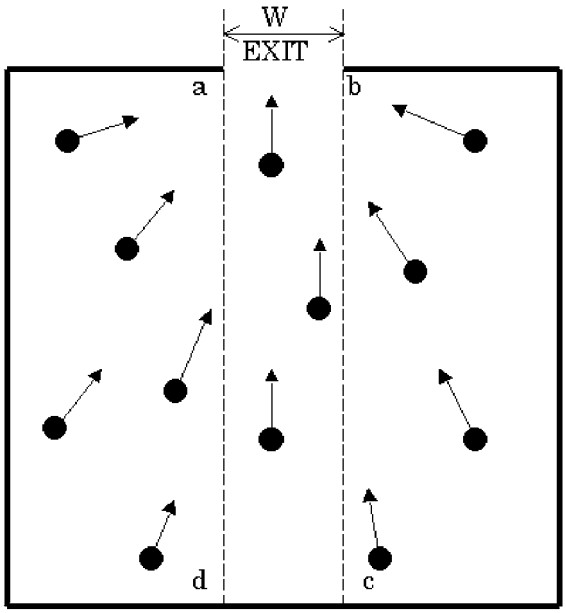

Figure 34. Schematic illustration of the crowd flow going, through the exit, outside the hall. A circle represents a walker. Each walker moves towards the exit without back step.

At the first stage ($0 < t < 30$), all walkers go towards to the exit. At the second stage ($30 \leqslant t < 200$), arching of walkers occurs since only a few walkers go, throughout the exit, outside the hall and almost all walkers cannot go out from the exist. At the third stage ($200 \leqslant t < 400$), the arching decays and flattening of walkers occurs by moving from the centre to both sides. At the fourth stage ($400 \leqslant t < 1500$), pitting appears above the exit. With increasing time, the depth of the pit becomes large. At the fifth stage ($t = 1500$), the bottom of the pit reaches to the neighbourhood of the exit. A hole is formed. At the sixth stage ($t > 1500$), the remaining walkers go out of the exit without clogging.

Figure 35 shows the plots of mean flow rate (current) J against time t for various values of door size W where hall length $L = 100$. The flow rate increases rapidly with time and saturates at $t = 30$. This saturation is due to the clogging of walkers at the exit. When the clogging occurs, only a few walkers go outside the hall with a constant value of mean flow rate. Then, the current decreases with time by forming the hole at the exit. In time, almost all walkers go outside the hall and the current approaches to zero. We find that a dynamical phase transition occurs from the clogging flow to the decaying flow.

In the clogging-flow region, the pedestrian flow exhibits the scaling behaviour. Figure 36 shows the log–log plot of the saturated flow rate J against door size W. The circular, triangular and square points indicate the simulation data for $L = 100$, 200 and 300, respectively. One finds that the saturated flow rate J scales as follows:

$$J \propto W^{0.88\pm0.02}, \tag{99}$$

where W is the door size at the exit.

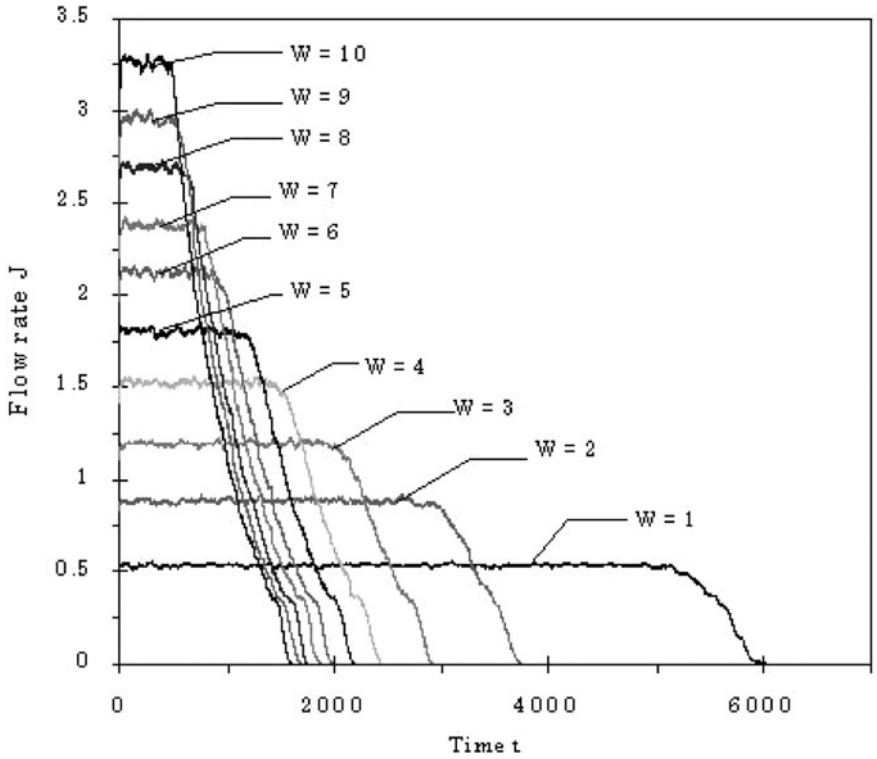

Figure 35. Plots of mean flow rate J against time t for door size $W = 1$–10 where hall length $L = 100$.

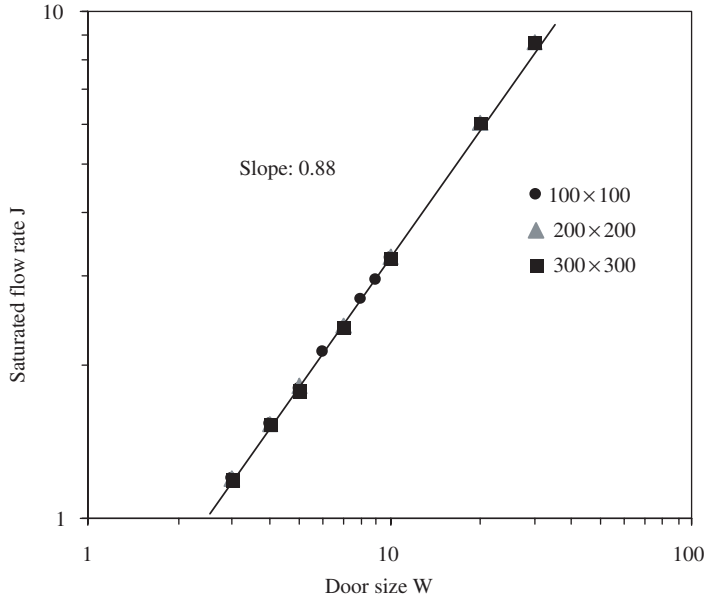

Figure 36. Log–log plot of saturated flow rate J_s against door size W where the circular, triangular and square points indicate the simulation data for $L = 100$, 200 and 300, respectively.

The scaling of the saturated flow has been found in the granular flow (Jaeger and Nagel 1996, Clement *et al* 2000). The scaling exponent 0.88 is less than 1.5 (2.5) in the two(three)-dimensional granular flow. Furthermore, the transition time from the clogging flow to the decaying flow exhibits the scaling behaviour. The transition time is given by the point changing from the saturated flow rate to the decreasing flow rate in figure 35. Figure 37 shows the log–log plot of transition time t_c against door size W. The circular, triangular and square points indicate the simulation data for $L = 100$, 200 and 300, respectively. One finds that the transition time t_c scales as

$$t_c \propto W^{-1.16\pm0.01}. \tag{100}$$

The transition time depends on the hall length L. The scaling exponent does not depend on L but the value of -1.16 is the same for the different L. This scaling has not been found in the granular flow. Based on the above scaling forms (99) and (100), we find that data collapses on a single line in the scaling region of the choking flow.

Helbing *et al* (2000a) have simulated the dynamical features of escape panic by using the generalized force model (94). They have found an optimal strategy for escape involving a mixture of individualistic behaviour and collective herding instinct.

7.4. Jamming transition

Pedestrians counteract the other in the channel of the subway or at the crossing where they come face to face. At a high density, pedestrians result in the jammed state, pile up and cannot move each other. The jamming transition occurs when the density of pedestrians is larger than the critical value. Muramatsu *et al* (1999) have found the jamming transition from the freely moving phase to the stopped (jammed) phase. Helbing *et al* (2000b) have also shown the similar jamming transition of 'freezing by heating'. Here, we explain the jamming transitions in the counter channel flow and at the crossing.

The counter flow model is described in terms of the lattice gas model with two components of particles. One component particle represents the walker going to the right and the other component particle represents the walker going to the left. Figure 38 shows the schematic illustration of the pedestrian counter flow in a channel. The right (left) walker is indicated by the full (open) circle. The channel is composed of length L and width W. The left and right boundaries are open. The density p_l (p_r) of the right (left) walker on the left (right) boundary is set by a constant value. When the right (left) walker arrives at the right (left) boundary, its walker is removed from the channel.

Figure 39(a) shows the plot of the mean velocity $\langle v \rangle$ against the entrance density $p(= p_l + p_r)$ for width $W = 10, 20, 50, 100, 200$ where $L = 500$ and $D = 0.0$. The mean velocity decreases slowly with increasing p. When the entrance density p is larger than the critical value p_c, the mean velocity becomes zero. Figure 39(b) shows the plot of the occupancy ρ against the entrance density p where the occupancy is defined as the fraction of sites occupied by the walkers. The occupancy increases sharply at the critical point p_c.

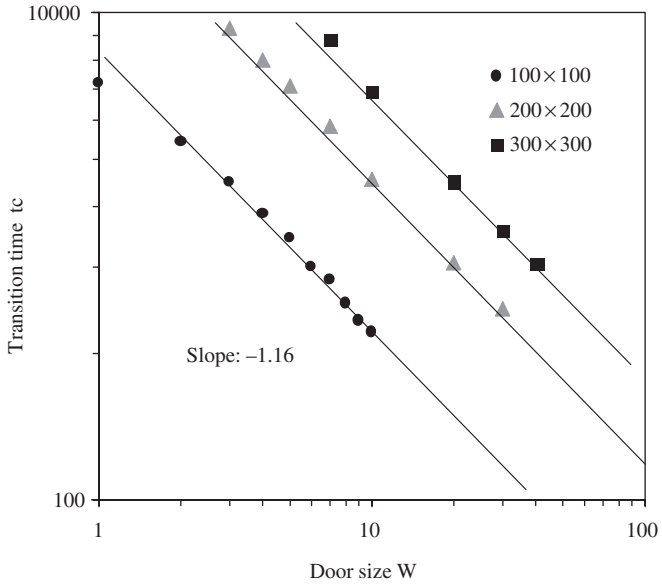

Figure 37. Log–log plot of transition time t_c against door size W where the circular, triangular and square points indicate the simulation data for $L = 100$, 200 and 300, respectively.

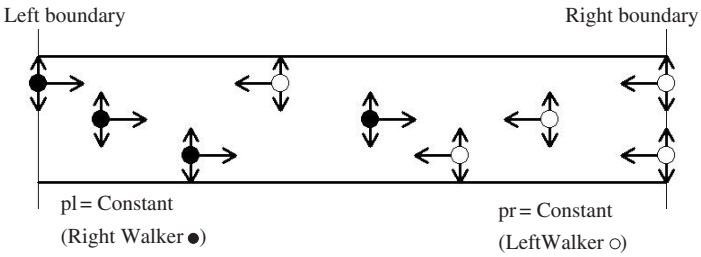

Figure 38. The schematic illustration of the pedestrian counter flow in a channel. The right (left) walker is indicated by the full (open) circle.

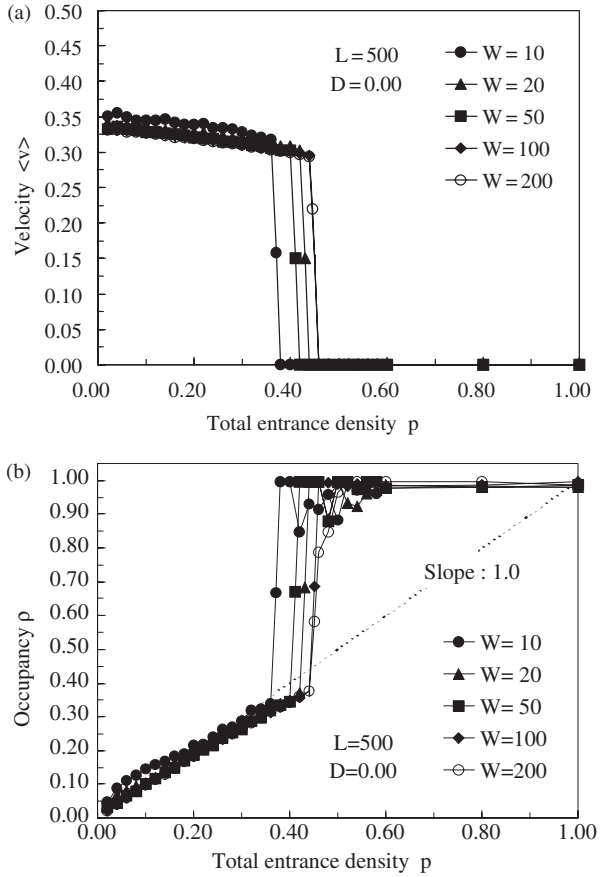

Figure 39. (*a*) The plot of the mean velocity $\langle v \rangle$ against the entrance density $p(= p_{\mathrm{l}} + p_{\mathrm{r}})$ for width $W = 10, 20, 50, 100, 200$. (*b*) The plot of the occupancy ρ against the entrance density p.

Thus, the jamming transition between the freely moving state and the jammed state occurs at the critical point. When the entrance density is superior than the critical point, the walkers counteract by going ahead of each other, they are piled up and are not able to move. The critical point approaches to $p_{\mathrm{c}} = 0.45$ when $W \to \infty$.

We consider the pedestrian flow at the square crossing connecting the four roads. In the pedestrian flow at the crossing, the jamming transition similar to the counter flow occurs when the total density is larger than the critical value. Figure 40 shows the schematic illustration of the pedestrian flow at the crossing under the open boundary condition. There are the four types of walkers. Each type of walkers has the desired direction different from each other. They do not change their desired direction. The model is described in terms of the lattice gas model with four components of particles.

The densities p_x, p_y, p_{-x}, p_{-y} of the right walker on the left boundary, the up walker on the bottom boundary, the left walker on the right boundary and the down walker on the up boundary are set at constant values, respectively. Figure 41(*a*) shows the plot of the mean velocity $\langle v \rangle$ against the total density p for the width $W = 20, 30, 50, 100, 200$ where, $p_x = p_y = p_{-x} = p_{-y}$ and $D = 0.0$. Figure 41(*b*) shows the plot of the occupancy ρ against the total entrance density p. When the entrance density is higher than the critical

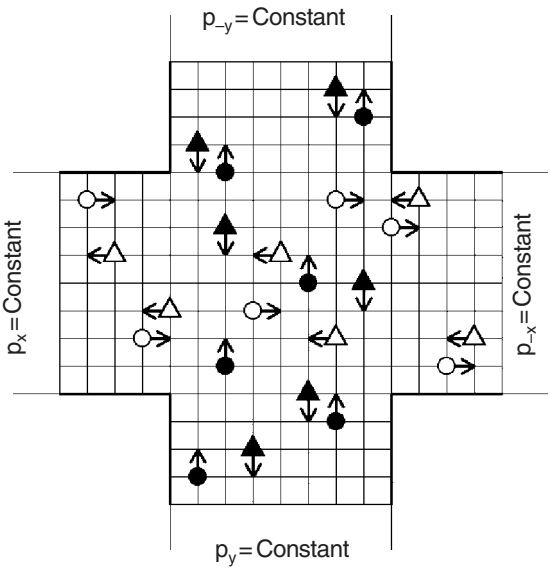

Figure 40. The schematic illustration of the four-way pedestrian flow at the crossing. The open (full) circles indicates the right (up) walker going to the right (up). The open (full) triangle indicates the left (down) walker going to the left (down).

value p_c, the mean velocity becomes zero and the occupancy increases steeply. The jamming transition between the moving phase and the stopped phase occurs at the critical density. The critical density $p_c = 0.45$ is obtained when $W \to \infty$. The critical value is consistent with that obtained in the counter flow. In the two-way flow at the crossing, the jamming transition occurs and the critical point agrees with that of the four-way flow (Muramatsu and Nagatani 2000c).

8. Summary

In this paper, we have shown that traffic systems display a surprisingly rich spectrum of spatio-temporal pattern formation phenomena. Although there are still many interesting open questions, one can state that traffic theory is a prime example of a mathematically advanced description of socio-physical systems.

From the point of view of statistical physics, one of the main aims of basic research on vehicular traffic is to understand the nature of the traffic jams. We have focused attention mainly on the progress made in the recent years using the car-following models. We have shown that the traffic jams are described mathematically in terms of the dynamical phase transitions and nonlinear waves. The typical nonlinear wave equations (the Burgers equation, the KdV equation and the modified KdV equation) are derived from the car-following model. Moreover, we have presented the generic phase diagram of the microscopic traffic model. We have explored that the jamming transition has properties very similar to the conventional phase transition and critical phenomenon even if the traffic system is far from equilibrium. The jamming transition is described by the TDGL equation.

We have also discussed the main models of traffic including the car-following models, the cellular automaton models, the gas-kinetic models and the fluid-dynamical models. The relationships between different approaches of modelling have been explored in detail. It has

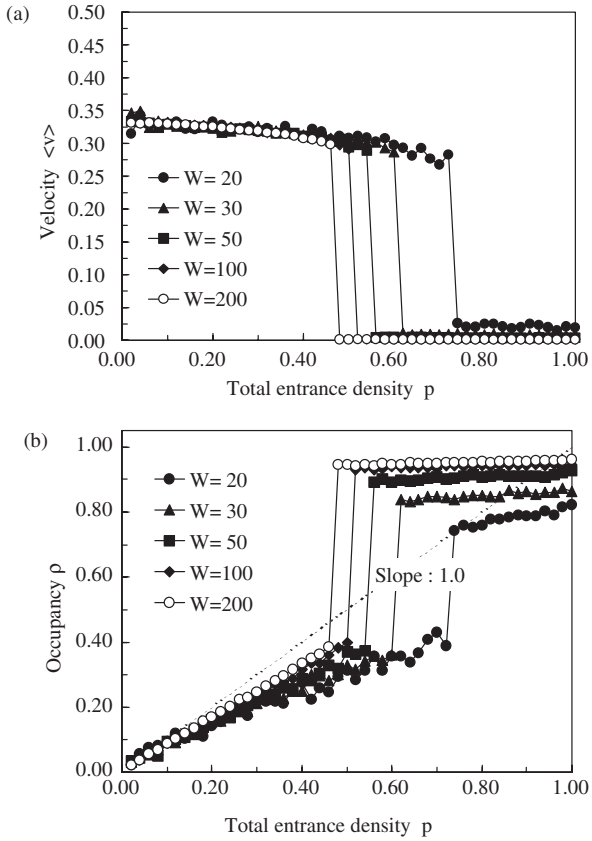

Figure 41. (*a*) The plot of the mean velocity $\langle v \rangle$ against the total density p for the width $W = 20$, 30, 50, 100, 200 where, $p_x = p_y = p_{-x} = p_{-y}$ and $D = 0.0$. (*b*) The plot of the occupancy ρ against the entrance density p.

been shown that the phenomenological parameters of the macroscopic theories can be estimated by utilizing the mathematical formulae relating these with those of the microscopic models.

The description of the phenomena in traffic systems uses and generalizes almost the complete spectrum of methods developed in nonequilibrium statistical physics and nonlinear dynamics. The motions of vehicles, buses and pedestrians have been described by Newton's equation of motion, complemented by driving forces and frictional dissipation. One has often found considerably different behaviour compared with analogous systems from classical mechanics, but there have also been various analogies to granular flow.

We have shown that the bus-route systems are modelled by the extended traffic models. The bunching transition between an inhomogeneous jammed phase (where the buses bunch together) and a homogeneous phase occurs with varying the initial time headway. The bunching of buses is closely connected to the Bose–Einstein-condensation-like phenomenon which has been observed in the particle-hopping models of traffic. We have also shown that the recurrent bus problem on a circular route is described mathematically in terms of the nonlinear map dynamics. The dynamics of the recurrent bus is closely related with the properties of the fixed points.

We have explored that the clogging transitions of pedestrian occur similarly to the traffic jams. The clogging of pedestrian is also similar to that of granular flow. The dynamic behaviour

exhibits the similarity to the asymmetric simple exclusion process. The pedestrian counter flow exhibits the jamming transition between the free flow and the stopped state. For practical applications to the evacuation process, a direct simulation of individual persons is important.

In order to predict the occurrence of a traffic jam at a specific place on a given highway at a particular instant of time, one not only needs more realistic models but also needs more detailed and accurate empirical data from real traffic.

Traffic is a good example to investigate the dynamical aspects of socio-physical phenomena. Traffic researches can help to obtain a better understanding of more complex human behaviour in the future.

Acknowledgments

I am grateful for the fruitful discussion with M Fukui, Y Ishibashi, M Bando, K Nakanishi, Y Sugiyama, S Tadaki, M Kikuchi, S Yukawa and H Emmerich. I would like to thank D Helbing, K Nagel, D E Wolf, M Schreckenberg and B S Kerner for supplying various figures.

References

Bando M, Hasebe K, Nakayama A, Shibata A and Sugiyama Y 1995a *Phys. Rev.* E **51** 1035
Bando M, Hasebe K, Nakanishi K, Nakayama A, Shibata A and Sugiyama Y 1995b *J. Phys.* I (France) **5** 1389
Barabasi A L and Stanley H E 1995 *Fractal Concepts in Surface Growth* (Cambridge: Cambridge University Press)
Barlovic R, Santen L, Schadschneider A and Schreckenberg M 1998 *Eur. Phys. J.* B **5** 793
Berg P, Mason A and Woods A 2000 *Phys. Rev.* E **61** 1056
Ben-Naim E and Krapivsky P L 1997 *Phys. Rev.* E **56** 6680
Ben-Naim E and Krapivsky P L 1998 *J. Phys.* A **31** 8073
Ben-Naim E and Krapivsky P L 1999 *Phys. Rev.* E **59** 88
Ben-Naim E, Krapivsky P L and Redner S 1994 *Phys. Rev.* E **50** 822
Biham O, Middleton A A and Levine D 1992 *Phys. Rev.* A **46** R6124
Cheybani S, Kertetz J and Schreckenberg M 2000 *Phys. Rev.* E **63** 016107
Chowdhury D and Desai R C 2000 *Eur. Phys. J.* B **15** 375
Chowdhury D, Santen L and Schadschneider A 2000 *Phys. Rep.* **329** 199
Clement E, Reydellet G, Rioual F, Parise B, Franguet V, Lanuza J and Kolb E 2000 *Traffic and Granular Flow '99* ed D Helbing, H J Herrmann, M Schreckenberg and D E Wolf (Berlin: Springer) p 457
Cross M C and Hohenberg P C 1993 *Rev. Mod. Phys.* **65** 851
Daganzo C F (ed) 1993 *Proc. 12th International Symp. on the Theory of Traffic Flow and Transportation* (Amsterdam: Elsevier)
Daganzo C F 1996 *Proc. 13th International Symp. on Transportation and Traffic Theory* ed J B Lesort (Tarrytown, NY: Pergamon) p 629
Daganzo C F 1997 *Fundamentals of Transportation and Traffic Operations* (Oxford: Pergamon–Elsevier)
Evans M R 1996 *Europhys. Lett.* **36** 13
Evans M R 1997 *J. Phys.* A **30** 5669
Fukui M and Ishibashi Y 1996 *J. Phys. Soc. Japan* **65** 1868
Fukui M and Ishibashi Y 1999 *J. Phys. Soc. Japan* **68** 2861
Gipps P G 1981 *Transpn Res.* B **15** 105
Greenshields B D 1935 *Proc. Highway Research Board* vol 14 (Washington, DC: Highway Research Board) p 448
Hall R W 1999 *Handbook of Transportation Science* (Boston: Kluwer)
Hall F L and Agyemang-Duah K 1991 *Transp. Res. Rec.* **1320** 91
Hayakawa H and Nakanishi K 1998 *Prog. Theor. Phys. Suppl.* **130** 57
Helbing D 1991 *Behav. Sci.* **36** 298
Helbing D 1995 *Physica* A **219** 391
Helbing D 1996a *Phys. Rev.* E **53** 2366
Helbing D 1996b *Physica* A **233** 253

Helbing D 1996c *Traffic and Granular Flow* ed D E Wlof, M Schreckenberg and A Bachem (Singapore: World Scientific) p 87
Helbing D 1997a *Verkehrsdynamik* (Berlin: Springer)
Helbing D 1997b *Phys. Rev.* E **57** 6176
Helbing D 1998a *A Perspective Look at Nonlinear Media. From Physics to Biology and Social Science* ed J Parisi, S C Muller and W Zimmermann (Berlin: Springer) p 122
Helbing D 1998b *Trafic and Granular Flow '97* ed M Schreckenberg and D E Wolf (Singapore: Springer) p 21
Helbing D 1998c *Phys. Rev.* E **57** 6176
Helbing D 2001 *Rev. Mod. Phys.* **73** 1067
Helbing D and Molnar P 1995 *Phys. Rev.* E **51** 4282
Helbing D and Molnar P 1997 *Self-Organization of Complex Structures: From Individual to Collective Dynamics* ed F Schweitzer (London: Gordon and Breach) p 569
Helbing D and Schreckenberg M 1999 *Phys. Rev.* E **59** R2505
Helbing D and Tilch B 1998 *Phys. Rev.* E **58** 133
Helbing D and Treiber M 1998a *Phys. Rev. Lett.* **81** 3042
Helbing D and Treiber M 1998b *Science* **282** 2001
Helbing D, Hennecke A and Treiber M 1999 *Phys. Rev. Lett.* **82** 4360
Helbing D, Farkas I J and Vicsek T 2000a *Nature* **407** 487
Helbing D, Farkas I J and Vicsek T 2000b *Phys. Rev. Lett.* **84** 1240
Henderson L F 1971 *Nature* **229** 381
Henderson L F 1974 *Transpn Res.* **8** 509
Henneke A, Treiber M and Helbing D 2000 *Traffic and Granular Flow '99* ed D Helbing, H J Herrmann, M Schreckenberg and D E Wolf (Berlin: Springer) p 383
Huijberts H J C 2002 *Physica* A **308** 489
Hurdle V F, Hauer E and Stewart G N (ed) 1983 *Proc. 8th International Symp. on Transportation and Traffic Flow Theory* (Toronto: University of Toronto)
Ispolatov I and Krapivsky P L 2000 *Phys. Rev.* E **62** 5935
Jaeger H M and Nagel S N 1996 *Rev. Mod. Phys.* **68** 1259
Janowsky S A and Lebowitz J L 1992 *Phys. Rev.* A **45** 618
Janowsky S A and Lebowitz J L 1994 *J. Stat. Phys.* **77** 35
Kauffman S 1995 *At Home in the Universe* (Oxford: Oxford University Press)
Kawasaki K 1984 *Ann. Phys.*, *NY* **154** 319
Kerner B S 1998 *Phys. Rev. Lett.* **81** 3797
Kerner B S 1999a *Phys. World* **12** 25
Kerner B S 1999b *Transpn Res. Record* **1678** 160
Kerner B S 2000 *Traffic and Granular Flow '99* ed D Helbing, H J Herrmann, M Schreckenberg and D E Wolf (Berlin: Springer) p 253
Kerner B S 2002 *Phys. Rev.* E **65** 046138
Kerner B S and Konhauser P 1993 *Phys. Rev.* E **48** R2355
Kerner B S and Konhauser P 1994 *Phys. Rev.* E **50** 54
Kerner B S and Rehborn H 1996a *Phys. Rev.* E **53** R1297
Kerner B S and Rehborn H 1996b *Phys. Rev.* E **53** R4275
Kerner B S and Rehborn H 1997 *Phys. Rev. Lett.* **79** 4030
Kerner B S, Konhauser P and Schilke M 1995 *Phys. Rev.* E **51** 6243
Kertész J and Kondor I 1998 *Econophysics: An Emerging Science* (Dordrecht: Kluwer)
Klar A and Wegener R 1999a *SIAM J. Appl. Math.* **59** 983
Klar A and Wegener R 1999b *SIAM J. Appl. Math.* **59** 1002
Klupfel H, Meyer-Konig T, Wahle J and Schreckenberg M 2000 *Theory and Practical Issues on Cellular Automata* ed S Bandini and T Worsch (London: Springer) p 63
Knospe W, Santen L, Schadschneider A and Schreckenberg M 2002a *Phys. Rev.* E **65** 056133
Knospe W, Santen L, Schadschneider A and Schreckenberg M 2002b *Phys. Rev.* E **65** 015101(R)
Komatsu T S and Sasa S 1995 *Phys. Rev.* E **52** 5574
Krauss S 1998 *Traffic and Granular Flow '97* ed M Schreckenberg and D E Wolf (Singapore: Springer) p 269
Krauss S, Wagner P and Gawron C 1996 *Phys. Rev.* E **54** 3707
Krauss S, Wagner P and Gawron C 1997 *Phys. Rev.* E **55** 5597
Krug J and Ferrari P A 1996 *J. Phys.* A **29** L465
Ktitarev D, Chowdhury D and Wolf D E 1997 *J. Phys.* A **30** L221
Kurtze D A and Hong D C 1995 *Phys. Rev.* E **52** 218

Lee H Y, Lee H-W and Kim D 1998 *Phys. Rev. Lett.* **81** 1130
Lee H Y, Lee H-W and Kim D 1999 *Phys. Rev.* E **59** 5101
Lee H Y, Lee H-W and Kim D 2001 *Phys. Rev.* E **64** 056126
Lehmann H 1996 *Phys. Rev.* E **54** 6058
Lighthill M J and Whitham G B 1955 *Proc. R. Soc.* A **229** 317
Lubashevsky I, Kalenkov S and Mahnke R 2002 *Phys. Rev.* E **65** 036140
Mahnke R and Pieret N 1997 *Phys. Rev.* E **56** 2666
Mantegna R N and Stanley H E 1999 *An Introduction to Econophysics* (Cambridge: Cambridge University Press)
Mason A D and Woods A W 1997 *Phys. Rev.* E **55** 2203
Meakin P 1998 *Fractals, Scaling and Growth Far from Equilibrium* (Cambridge: Cambridge University Press)
Muramatsu M and Nagatani T 1999 *Phys. Rev.* E **60** 180
Muramatsu M and Nagatani T 2000a *Trans. Japan Soc. Mech. Eng.* **66** 2884 (in Japanese)
Muramatsu M and Nagatani T 2000b *Physica* A **275** 281
Muramatsu M and Nagatani T 2000c *Physica* A **286** 377
Muramatsu M, Irie T and Nagatani T 1999 *Physica* A **267** 487
Musha T and Higuchi H 1976 *Japan. J. Appl. Phys.* **15** 1271
Musha T and Higuchi H 1978 *Japan. J. Appl. Phys.* **17** 811
Nagatani T 1995 *Phys. Rev.* E **51** 922
Nagatani T 1996 *J. Phys. Soc. Japan* **65** 3150
Nagatani T 1997a *Physica* A **237** 67
Nagatani T 1997b *J. Phys. Soc. Japan* **66** 1219
Nagatani T 1997c *J. Phys. Soc. Japan* **66** L1928
Nagatani T 1998 *Phys. Rev.* E **58** 4271
Nagatani T 1999a *Phys. Rev.* E **60** 6395
Nagatani T 1999b *Physica* A **264** 581
Nagatani T 1999c *Phys. Rev.* E **59** 4857
Nagatani T 2000a *Phys. Rev.* E **61** 3534
Nagatani T 2000b *Physica* A **280** 602
Nagatani T 2000c *Phys. Rev.* E **61** 3564
Nagatani T 2000d *Physica* A **287** 302
Nagatani T 2001a *Phys. Rev.* E **63** 036115
Nagatani T 2001b *Physica* A **296** 320
Nagatani T 2001c *Physica* A **297** 260
Nagatani T 2001d *Physica* A **300** 558
Nagatani T, Nakanishi K and Emmerich H 1998 *J. Phys.* A **31** 5431
Nagel K and Herrmann H J 1993 *Physica* A **199** 254
Nagel K and Paczuski M 1995 *Phys. Rev.* E **51** 2909
Nagel K and Schreckenberg M 1992 *J. Phys.* I (France) **2** 2221
Nagel K, Wolf D E, Wagner P and Simon P 1998 *Phys. Rev.* E **58** 1425
Nagel K, Esser J and Rickert M 1999 *Ann. Rev. Comp. Phys.* ed D Stauffer (Singapore: World Scientific)
Nakanishi K, Itoh K, Igarashi Y and Bando M 1997 *Phys. Rev.* E **55** 6519
Nakayama A, Sugiyama Y and Hasebe K 2002 *Phys. Rev.* E **65** 016112
Nelson P 2000 *Phys. Rev.* E **61** R6052
Neubert L, Santen L, Schadschneider A and Schreckenberg M 1999 *Phys. Rev.* E **60** 6480
Newell G F 1961 *Oper. Res.* **9** 209
Nishinari K 2001 *J. Phys.* A **34** 10727
Nishinari K and Takahashi D 2000 *J. Phys.* A **33** 7709
O'loan O J, Evans M R and Cates M E 1998 *Phys. Rev.* E **58** 1404
Paveri-Fontana S L 1975 *Transpn Res.* **9** 225
Payne H J 1971 *Mathematical Models of Public Systems* vol 1, ed G A Bekey (La Jolla, CA: Simulation Council) p 51
Payne H J 1979 *Transpn Res. Rec.* **722** 68
Phillips W F 1979 *Transpn Plan. Technol.* **5** 131
Popkov V and Schutz G M 1999 *Europhys. Lett.* **48** 257
Prigogine I and Andrews F C 1960 *Oper. Res.* **8** 789
Prigogine I and Herman R 1971 *Kinetic Theory of Vehicular Traffic* (New York: Elsevier)
Schadschneider A 2001 *Pedestrian and Evacuation Dynamics* ed M Schreckenberg and D Sharma (Berlin: Springer) p 75
Schadschneider A and Schreckenberg M 1993 *J. Phys.* A **20** L679

Schadschneider A and Schreckenberg M 1997a *Ann. Physik* **6** 541
Schadschneider A and Schreckenberg M 1997b *J. Phys.* A **30** L69
Schmittmann B and Zia R K P 1998 *Phys. Rep.* **301** 45
Schreckenberg M and Sharma D (ed) 2001 *Pedestrian and Evacuation Dynamics* (Berlin: Springer)
Schreckenberg M, Schadschneider A, Nagel K and Itoh N 1995 *Phys. Rev.* E **51** 2939
Shvetsov V and Helbing D 1999 *Phys. Rev.* E **59** 6328
Spohn H 1991 *Large Scale Dynamics of Interacting Particles* (Berlin: Springer)
Schutz G M 2000 Exactly solvable models for many-body systems far from equilibrium *Phase Transitions and Critical Phenomena* vol 19, ed C Domb and J Lebowitz (London: Academic)
Stanley H E 1971 *Introduction to Phase Transitions and Critical Phenomena* (Oxford: Oxford University Press)
Stanley H E and Ostrowsky N 1986 *On Growth and Form* (Boston: Martinus Nijhoff)
Sugiyama Y, Nakayama A and Hasebe K 2001 *Pedestrian and Evacuation Dynamics* ed M Schreckenberg and D Sharma (Berlin: Springer) p 155
Tadaki S, Kikuchi M, Sugiyama Y and Yukawa S 1998 *J. Phys. Soc. Japan* **67** 2270
Tajima Y, Takimoto K and Nagatani T 2001 *Physica* A **294** 257
Tajima Y and Nagatani T 2001 *Physica* A **292** 545
Takayasu M and Takayasu H 1993 *Fractals* **1** 860
Tatsumi T and Kida S 1972 *J. Fluid Mech.* **55** 659
Tomer E, Safonov L and Havlin S 2000 *Phys. Rev. Lett.* **84** 382
Treiber M, Henneke A and Helbing D 1999a *Traffic and Granular Flow '99* ed D Helbing, H J Herrmann, M Schreckenberg and D E Wolf (Berlin: Springer) p 365
Treiber M, Hennecke A and Helbing D 1999b *Phys. Rev.* E **59** 239
Treiber M, Hennecke A and Helbing D 2000 *Phys. Rev.* E **62** 1805
Treiterer J and Taylor J I 1966 Traffic flow investigations by photogrammetric techniques *High. Res. Rec.* **142** 1
Treiterer J and Myers J A 1974 *Proc. 6th International Symp. on Transportation and Traffic Theory* ed D Buckley (London: Reed) p 13
Vicsek T 1992 *Fractal Growth Phenomena* 2nd edn (Singapore: World Scientific)
Wagner C 1997 *Physica* A **245** 124
Wagner C 1998 *J. Stat. Phys.* **90** 1251
Wagner C, Hoffmann C, Sollache R, Wagenhuber J and Schurmann B 1996 *Phys. Rev.* E **54** 5073
Whitham G B 1990 *Proc. R Soc.* A **428** 49
Wiedemann R 1995 *Beitrage zur Theorie des Strassenverkehrs* ed H Keller (Koln: Forschungsgesellshaft fur Strassen- und Verkehrswesen)
Wolf D E 1999 *Physica* A **263** 438
Wolfram S 1986 *Theory and Applications of Cellular Automata* (Singapore: World Scientific)
Wolfram S 1994 *Cellular Automata and Complexity* (Reading, MA: Addison-Wesley)
Yukawa S and Kikuchi M 1995 *J. Phys. Soc. Japan* **64** 35